INVESTIGATING THE BINDING CAPABILITIES OF TRIAZOLE-CALIX[4]ARENE FUNCTIONALIZED MICROCANTILEVER SENSORS TOWARDS HEAVY METALS IN AQUEOUS SOLUTION

by © Mona Braim A Thesis submitted

to the School of Graduate Studies in partial fulfillment of the

Requirements for the degree of

MSc in Physics

Department of Physics and Physical Oceanography

Faculty of Science

Memorial University of Newfoundland

March, 2017

St. John's Newfoundland

Abstract

The main objective of this work was to investigate the binding capabilities of gold-coated micro-cantilever sensors functionalized with a bimodal triazole-calix[4]arene towards select heavy metals (e.g. Hg^{2+}, Fe^{3+}, Ni^{2+}, Zn^{2+}, and Pb^{2+}). The interaction between the triazole-calix[4]arene functionalized micro-cantilevers and the target analytes resulted in the formation of a differential surface stresse, which in turn, resulted in a mechanical deflection of the microcantilever. Results showed that microcantilever arrays modified with triazole-calix[4]arene were capable of detecting trace concentrations of Hg^{2+} ions as low as 10^{-11} M, which is sufficiently low for most applications. Results also showed that triazole-calix[4]arene functionalized microcantilevers were capable of detecting the presence of Pb^{2+} ions in aqueous solution of Hg^{2+}.

A new functionalization unit was also constructed to functionalize all 8 microcantilevers in an array with different sensing layers simultaneously, thus increasing the accuracy and reliability of the experimental results.

Key terms: Microcantilever sensor; MCL; functionalization unit; heavy metal toxicity; calixarenes; deflection; Mercury; triazole-calix[4]arene

Acknowledgements

First and foremost, I would express my wholehearted thanks to my beloved parents Mohammed & Norah, without whose vision this would have been only a dream, also to my brothers and sisters for their endless love, unwavering support, and encouragement as I went through this journey.

I acknowledge, with sincere gratitude, my supervisor Dr. Luc Beaulieu for giving me the opportunity to work on this interesting topic. Without his guidance, help, support, and patience I would not have made headway in this project.

I am lucky to have the opportunity to work with such a wonderful group of professionals from both the Physics and Chemistry Departments. This project would not have been possible if we had not come together and collaborated. Every single person in our group made a significant contribution, but some stand out in particular as deserving of outstanding praise.

Prof. Paris E. Georghiou provided thoughtful comments and many helpful discussions and Dr. Shofiur Rahman who constantly welcome me every time in spite of his busy schedule, provided insightful guidance, advice, and great efforts to explain things simply and clearly, and I really appreciate all they contributed.

Dr. Abdullah Alodhayb's explanations and his expert input on the labs instrumentations were invaluable while working on my project. His practical lab tips and the guidance he provided were incredibly helpful and he deserves recognition for all his help. Working with

Hanin Algaidi in the lab was a great experience and I thank her for her helpful discussions and her sunny cheerfulness.

I would also like to sincerely thank my friends Ameera Alrashdi and Suhad Sbeih whose strong words of encouragement on-line gave me the energy and motivation to complete this research and get the most out of this wonderful period of my life.

Without the Ministry of Higher Education, Kingdom of Saudi Arabia and its generous scholarship support, I would not be where I am today. This work was also supported in parts by Memorial University, NSERC, RDC, and Vale. Special thanks go to the Saudi Arabian Cultural Bureau in Canada for their continued guidance and facilitation throughout my full period of study.

Table of Contents

List of Tables

List of Figures

List of Symbols and Abbreviations

Ar	Argon
AAS	Atomic absorption spectroscopy
AFM	Atomic force microscopy
NH_4OH	Ammonium hydroxide
Φ	Azimuthal angle
Δm	Change in mass
DNA	Deoxyribonucleic acid
$Hg(CH_3)_2$	Dimethyl mercury
D	Distance between the incident beam and the microcantilever base
L	Distance between the incident beam on a MCL and the PSD
Au	Gold
HIV	Human immunodeficiency virus
HF	Hydrofluoric acid
HCl	Hydrogen chloride
H_2O_2	Hydrogen peroxide
Θ	Angle of inclination
ISE	Ion-selective electrode
MCLs	Microcantilever
CL	Microcantilever length

t	Microcantilever thickness
M	Molar concentration = mol /L
OBDS	Optical beam deflection system
v	Poisson's ratio
PSD	Position sensitive photodiode
KOH	Potassium hydroxide
ζ	PSD angle
f	Resonance frequency
SAM	Self-assemble monolayer
Si	Silicon
SiO_2	Silicon dioxide
Si_3N_4	Silicon nitride
k	Spring constant
H_2SO_4	Sulfuric acid

Co-authorship Statement

This statement is written to outline the contributions to this work by different members of our group. Mona Braim conducted all the experiments presented in this thesis, unless otherwise stated. Abdullah Alodhayb and Saydur Rahman made the majority of the contributions to the design of the experimental setup discussed in Chapter 3. The synthesis of the chemical compounds described in this thesis was performed in the laboratory of Dr. Paris Georghiou in the Department of Chemistry, Memorial University. With regards to the results outlined in Chapter 4 also published in [1], I prepared and conducted the experiments and actively participated in the analysis of the experimental data. I participated in the manuscript preparation through discussion and suggestions of the subsequent revisions to the manuscript which was originally written by others. The improvements to the functionalization unit (i.e. Chapter 6) to allow eight microcantilevers to be functionalized simultaneously (instead of four) were done by me.

Chapter 1 Introduction

1.1 Background

Water is an essential substance for all life forms on the planet. Monitoring water supplies is of paramount importance for the safety of people, the environment, and for organisms living in our ecosystems. Developments in agriculture and industrial activities have led to a substantial increase of pollutants and contaminants in the environment and especially freshwater supplies [2]. Some of these pollutants are heavy metals whose presence in fresh water has caused growing concern due to the health issues associated with these metals [2].

1.2 Statement of Problem

Owing to the pernicious effects of heavy metals on human health and the ecosystem, there is an urgent need to monitor and control these hazardous pollutants. As a result of increasing environmental consideration numerous analytical methods have been developed [3]. The growing demand for water quality monitoring has directed a substantial amount of effort towards the development of sensing-based devices capable of detecting trace concentrations of heavy metals in fresh water [4,5].

1.3 Objectives

Our research has two primary objectives.

1.3.1 Objective for Part I

The first part of this dissertation focuses on the primary objective of investigating the binding capabilities of the newly synthesized triazole-calix[4]arene towards Hg^{2+}, Fe^{3+}, Ni^{2+}, Zn^{2+} and Pb^{2+} in aqueous solutions.

1.3.2 Objective for Part II

The second part of this dissertation focuses on the development of a new functionalization system to simultaneously functionalize eight different microcantilevers (MCLs) within an array, with different sensing layers individually.

1.4 Thesis Outline

Part I begins with Chapter 2, which is a literature review. The literature review begins with a discussion of heavy metals, including mercury, lead and nickel. It outlines the regulations for safe limits of heavy metals in freshwater sources in Canada. Next, it provides an overview of the technology that is currently available for detection heavy metals—including atomic absorption spectroscopy, ion-selective electrode, and MCL sensors—as well as their limitations. The literature review continues with a more in depth focus on MCL Sensors, which is the technology used in our research. The literature review concludes with a brief overview of calixarenes produced by Dr. Georghiou's research group.

Chapter 3 describes the methodology employed in this work. The methodology begins by outlining the MCL surface functionalization, including proper cleaning techniques and thin film deposition. The methodology continues by detailing our experimental setup, including each major component of the set up. After briefly addressing our delimitations, the methodology outlines our experimental procedures and our data collection methods.

Chapter 4 provides our results and discussion, focusing first on the effect of concentration variation on the deflection produced by the triazole-calix[4]arene functionalized MCLs and then analysing the effects of the presence of other metal ions. Our discussion concludes with an investigation of the effect of cations on the sensitivity of the triazole-calix[4]arene functionalized MCLs.

Part II begins with Chapter 5. This chapter introduces other methods of functionalizing MCLs than the one used in our methodology for Part I. A description of the original functionalized unit developed in our group is presented, followed by a complete description of the new functionalization unit capable of functionalizing eight MCLs simultaneously each with a different sensing layer.

Chapter 6 presents our conclusions and suggests directions for future research. It provides a summary of our contributions to the literature and new research presented in this dissertation.

Part I

Chapter 2 Literature Review

2.1 Heavy Metals

There have been debates regarding the definition of heavy metals and the classification of elements that belong to it [6]. One of the most common definitions is metals that have eco-toxic properties [6] and have a relative density between 4.5 g/cm^3 and 22.5 g/cm^3 [6,7]. Anthropogenic activities (i.e. mining activities and industrial production [8]) and some natural processes (i.e. acid rain [9], leaching of rocks, and forest fires [10]) result in the accumulation of heavy metals in the environment [8].

2.1.1 Heavy Metal Toxicity

Mercury (Hg), iron (Fe), cadmium (Cd), zinc (Zn), nickel (Ni), copper (Cu), and lead (Pb) are some examples of the most common heavy metals found in the environment. Some heavy metals are important for the proper functioning of the human body and for biochemical processes [8,11,12]. For example, the recommended dietary allowance of both iron [13] and zinc [14] is 8 mg/day for adolescents aged 9-13, in order to meet their nutritional needs. However, other heavy metals such as mercury, lead, and cadmium are toxic for living organisms even at low concentrations and can be very harmful [9].

Their toxic effects on human health and aquatic biota have been reported [9] with disasters occurring not only recently but repeatedly for many decades, throughout the world. Some notable examples include: the official discovery of Minamata Disease in 1956 which is a severe mercury poisoning [15] leading to a neurological and congenital disease caused by the bioaccumulation of methylmercury in aquatic organisms and food sources in Minamata Bay in Japan [16]; the immense water supply contamination by lead in Picher, Oklahoma in 1967 [17]; the Bhopal industrial pesticide disaster in India in 1984 [18]; the devastating Basel industrial chemical storehouse fire in Switzerland in 1986 [19]; the mineral waste contamination of the River Guadiamar basin in Seville, Spain in 1998 [20]; the severe cyanide and heavy metal (Pb, Cd, Cu, and Zn) contamination of the rivers Szamos in Hungary from the release of toxic sludge from a Gold processing plant in 2000 [21]; the significant leak in the gypsum pond of Talvivaara Mining Company's Nickle & Zinc mine in eastern Finland in 2012 [22]; the devastating breach of tailings pond at the Mount Polley mine in British Columbia in 2014 [23]; and, the failure of the U.S. Environmental Protection Agency when it accidentally released contaminated wastewater from the Gold King mine [23] in Colorado, USA while on site to address contaminations in 2015 [24]. These are only some examples of the many devastating toxic disasters related to heavy metals being present in close proximity to human beings, even in trace amounts.

2.1.2 Mercury

Mercury is one of the most toxic metals [24,25] and its harmful effects on living organisms and the environment are commonly known [15]. Mercury is a natural constituent of the

Earth's crust that can be detected in air, water, and soil. A variety of anthropogenic sources, including dental offices [26], are responsible for the presence of mercury in wastewater treatment plants and the environment (Figure 2.1). For instance, industrial activities such as metal mining, fossil-fuel combustion, and chemical industrial production significantly increase the presence of mercury in the environment [12,27].

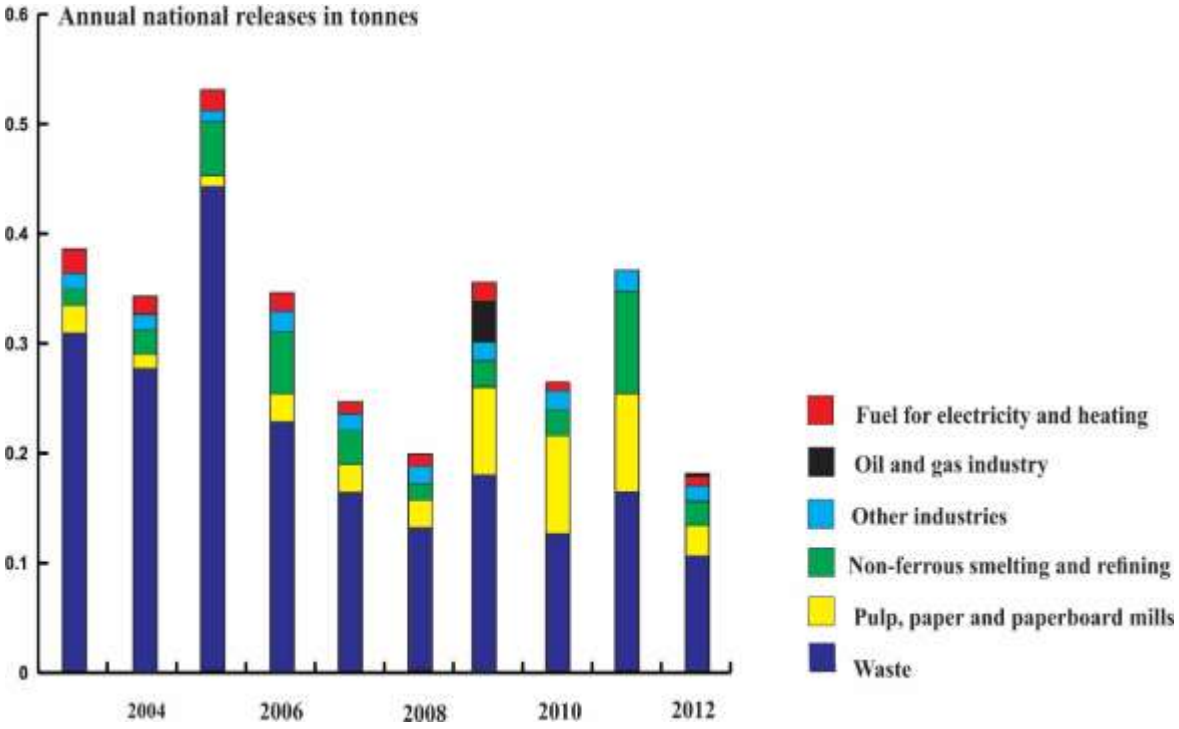

Figure 2.1: An illustration of mercury released into Canadian water by different sources from 2003-2012. © Her Majesty the Queen in Right of Canada, as represented by the Minister of the Environment, 2014 http://www.ec.gc.ca. This figure is adapted with permission from Figure 5 in [26].

Mercury exists in different poisonous forms; organic, inorganic, and elemental mercury [28]. Mercury is converted into methylmercury $[CH_3Hg]^+$, which is the most toxic organic form of mercury, through a methylation process by microorganisms [29]. Human intake of mercury in its various forms most often occurs through either dermal contact with elemental mercury, inhalation of mercury vapour, or ingestion of fish that have high levels of methylmercury [15,30]. The consumption of contaminated vegetation by fish and other aquatic organisms, leads to bioaccumulation and the migration of mercury-based contaminants to other animals throughout the food chain [15,30]. Numerous studies indicate that mercury exposure can have severe effects on living organisms, including on unborn fetuses [12,16,27,29]. The most common symptoms related to methylmercury poisoning such as Minamata disease include tremors, sensory disturbances, constriction of the visual field, and auditory disturbances, among many others [16]. The impact of a fetus poisoned as a result of their mother's ingestion of contaminated food is even more severe, including brain lesions, cerebral atrophy, mental retardation, deformity of limbs, and many other physical and neurological symptoms [16]. High level exposure can have detrimental effects on nearly all body systems, including the nervous, cardiovascular, respiratory, excretory, digestive, hepatic, and muscular system [31].

2.1.3 Lead

Lead is another example of a heavy metal that is a naturally occurring element in the environment. Lead accumulates in the environment over a period of years and is released as a result of natural sources and human activities such as waste oil disposal, burning fossil

fuels, and smelting activities [32]. Respiration in a contaminated environment and ingestion of polluted water or other food items are the main sources of lead poisoning in humans and animals [12]. Children are most vulnerable [12,33] to lead poisoning, which impairs their cognitive and behavioural development [33]. Lead poisoning can cause devastating health consequences including neurological damage [33,34], cerebrovascular disease, hypertension, skeletal changes, gastrointestinal symptoms, heart disease, cancer, and in some cases, death [34].

2.1.4 Nickel

Another example of a toxic heavy metal is nickel, which exists naturally in the Earth's crust in several mineral forms [35]. It has numerous applications including metallurgical processes and industrial plumbing [36]. Although nickel is a crucial element in low amounts (i.e. <1 mg/day) for mammalian species and can be included in human nutrition [35], consumption of high doses of nickel (i.e. >0.5 g/day) can negatively affect human health as well as that of fish, birds, and amphibians [35]. Nickel is released into the environment as a result of many anthropogenic activities such as mining and alloy processing [37]. Exposure to refined nickel dust can cause lung and nasal cancer [38]. Humans are exposed to nickel from a variety of sources such as air, food, and contaminated water [37]. Consumption of contaminated water can result in hazardous health problems such as damage to lungs and kidneys [35].

2.1.5 Safe Limits

Even in trace amounts, the presence of some heavy metals in fresh water and the environment can have drastic effects on life forms. The safe limit for different heavy metals varies, as some metals are toxic at very low concentrations and others only at higher concentrations. The recommended permissible limits in Canada for heavy metals in fresh water is displayed in Table 2.1.

Table 2.1: Permissible concentrations of different heavy metals in fresh water as suggested by the Canadian water quality guidelines for the protection of aquatic life. Adapted from Canadian water quality guidelines for the protection of aquatic life [39].

Metal	Chemical Symbol	(µg/L)
Lead	(Pb)	< 1-7.0
Mercury	(Hg)	< 0.026
Nickel	(Ni)	< 25-150
Iron	(Fe)	< 300
Zinc	(Zn)	< 30

2.2 Conventional Techniques for Analysis of Heavy Metals

There is a wide variety of technology that is currently available on the market that can be used to analyze samples for heavy metals, among other applications.

2.2.1 Atomic Absorption Spectroscopy (AAS)

Atomic absorption spectroscopy (AAS) has the ability to identify numerous metal elements by measuring their concentration [40]. AAS is based on the principle of atomic absorption of specific frequencies when they pass through a sample [40]. By measuring the amount of radiation absorbed by a substance, the target atom concentration can be determined [40]. The AAS technique is relatively easy to use and inexpensive [40], however it has some drawbacks. It can be used only for aqueous analysis, it is capable of determining only one element at a time [40], the samples should have specific properties (i.e. colourless and transparent), large sample quantities are required, and the protocol of the sample preparation is a long process [40].

2.2.2 Ion-Selective Electrode (ISE)

Ion-selective electrode (ISE) is another analytical technique that is widely used for measuring the concentrations of various ions in aqueous solutions [41]. ISE consists of inner and outer electrolyte solutions, two equal reference electrodes, and a permeable ion selective membrane for a single ion type [42]. The theory behind ISE focuses on measuring the electrical potential difference generated when the desired ionic species transfers from the higher potential solution to the lower one through the membrane [41]. By determining this potential difference, the ionic activity of the analyte can be estimated [41,42]. The ISE

technique has *in-situ* analysis capabilities and it is cost-effective and easy to operate [41]. However, this technique has unavoidable limitations such as interference effects from other ions in the aqueous solution, and the inconvenience of having to change the membrane each time a new target ion is measured [41]. Additionally, this technique is limited to detecting only ions with specific charge densities [43], and suffers from low accuracy due to the potential drift in the reference electrode, which occurs when the concentration varies in different areas within a highly concentrated solution [44].

2.2.3 Microcantilever (MCL) Sensors

Another monitoring technology is Microcantilever (MCL) sensors, which have been effectively employed in proof-of-purpose applications in a wide range of physical, chemical, and biological applications [45]. Some applications in the medical field include the screening of diseases such as viral infections [46], HIV [47], and cancer [48]. In terms of physical applications, MCL sensors have been applied for the detection of temperature [49], surface stress [50], and changes in mass [51]. Biological and chemical applications include the detection of DNA hybridization, antigen-antibody interactions [52], explosives [53], and metal ions [54].

At its most basic level, MCL sensors are devices that consist of a recognition element and transducer that is used to convert physical properties such as temperature or chemical properties such as ion concentration, into measurable electrical signals [55,56]. MCL sensors can be used to detect diverse trace substances and can be operated in various environments (i.e. gaseous, vacuum, or liquid medium), giving them a wide variety of

possible applications [56,57]. Different problems can be addressed with this technology as it is not limited to a single application. One major limitation of MCLs is that their various sensing abilities and the underlying mechanisms governing their behavior are not well understood, despite a significant amount of analytical and numerical research conducted [58,59,60]. As a result of this incomplete understanding of MCLs, they lack accessibility and are not used in commercial applications [60].

2.2.4 Limitations of Current Techniques

Despite the fact that the conventional analytical instruments offer adequate limits of detection [5], they can be time consuming to use due to the sample preparation and the need for highly trained operators, require regular maintenance [5,57], and are too complicated to be available on the market for common use.

In comparison, MCLs have fewer limitations than the other analytical techniques described. Use of MCL sensors as an analytical technology has several advantages over other conventional techniques in the terms of simplicity, high sensitivity, versatility, ease of use, and rapid response [61].

2.3 Detailed Overview of MCLs

A MCL sensor is composed of three main components: a cantilever, recognition layer, and optical beam deflection system (OBDS). The cantilever is a micrometer-sized silicon lever that acts like as transducer [62]. The recognition layer is a key component that is most often composed of a self-assembled monolayer functionalized with a receptive end group. The

recognition layer is constructed so that target analytes of interest bind preferentially to the probe molecules. The interaction between the receptive layer and the target analyte are detected using an OBDS, which is the third component of the sensor. The OBDS consists of an optical beam which is reflected off the free end of the cantilever into a position sensitive detector. As the cantilever bends, the position of the optical beam on the detector changes creating a measurable signal which can be used to obtain the amount that the cantilever deflected.

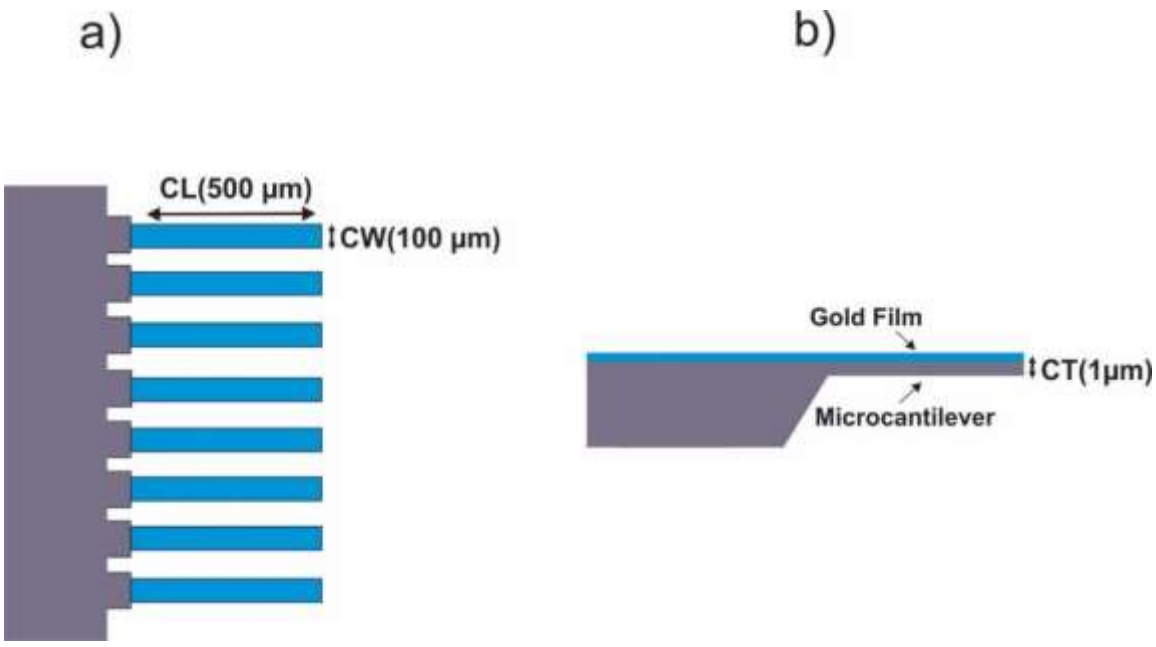

Figure 2.2: A schematic representation of a) an MCL array from the top and b) a side view of an MCL with a gold film deposited on the top surface side. The CLA500-010-08l MCL array has individual MCLs with dimensions of CL = 500 µm, CW = 100 µm, and CT = 1 µm.

A single MCL is a beam clamped at one end and free at the other. In this work, commercially available arrays of 8 rectangular silicon MCL[1] (Figure 2.2a), with typical dimensions of 500 µm long, 100 µm wide, and 1µm thick, were used. The MCLs are chemically activated by coating one side with a thin gold film (Figure 2.2b), upon which a chemical receptor is immobilized. When a target molecule of interest interacts with the receptor, a surface stress is generated, causing a nano-mechanical deflection to occur in the MCL. This deflection can be monitored using an OBDS [63]. The underside of MCLs can be left unfunctionalized or coated with a passivation layer to prevent competing reactions from occurring and affecting the measurements [64].

2.3.1 MCL Fabrication Process and Sensor Material

MCLs are most often fabricated from either silicon (Si), silicon nitride (Si_3N_4), or polymers, using micromachining processes such as bulk micromachining. The bulk micromachining fabrication process consists of different steps including substrate preparation, MCL patterning, and device release [65].

In the first step as shown in Figure 2.3a, a thin layer of the material composing the MCL, called the device layer (signified in orange), is deposited over an etch stop layer (signified in green), which is deposited on the silicon wafer (signified in purplish blue). The etch stop layer is used to protect the device layer during the etching process. In the second step, the

[1] CLA500-010-08l, Concentris, GmbH, Switzerland

MCL is defined by using photoresist (signified in purple) to pattern the shape of the device (cantilever) [65,66] (Figure 2.3b). This step is followed by the chemical process of wet etching which is isotropic in the device layer and directional in the silicon substrate on the back side of the MCL [67] (Figure 2.3c). Finally, etching the etch stop results in the production of the MCL device [68], as shown in Figure 2.3d.

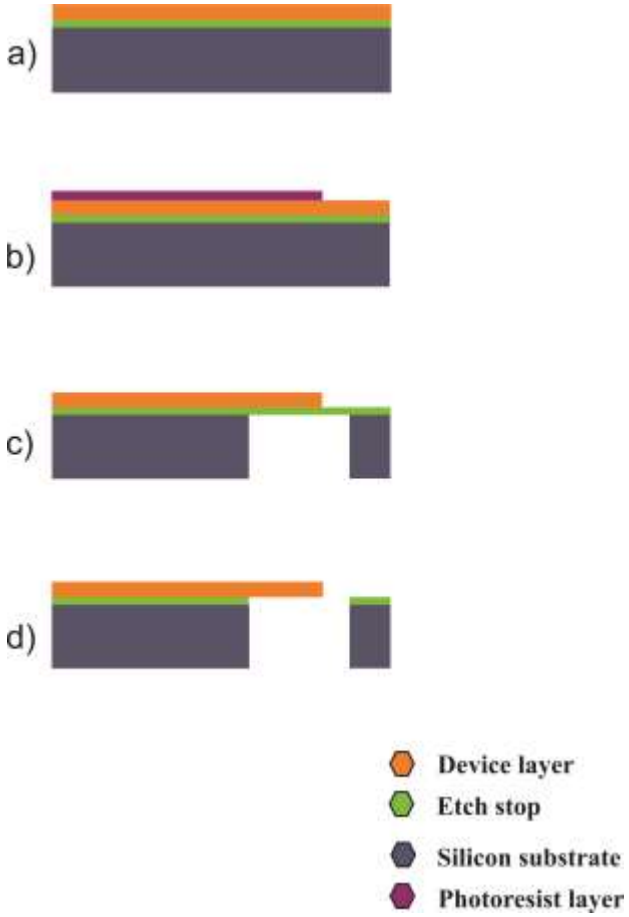

Figure 2.3: An illustration of the different steps of the bulk micromachining process used to fabricate silicon MCLs. The device layer (in orange), the etch stop layer (in green), and the silicon substrate (in purplish blue) together form the structure of the MCL.

2.3.2 MCL Principles of Operation

MCL sensors have two major modes of operation: static mode and dynamic mode, which differ based on the type of measurement to be performed [69,70]. Depending on the mode, the MCLs are able to perform measurements using either one or both sides, and so the MCL surface needs to be uniformly coated on just one side (for static mode) or both sides (for dynamic mode) [70,71]. The static mode measures change in surface stress and so it is ideal for vacuum, gaseous and liquid mediums. On the other hand, the dynamic mode measures change in vibrational frequency and so while it is extremely effective under vacuum or ambient conditions, the viscous damping of the surrounding medium prevents this mode from being used in liquid [71,72]. In the static mode, it is preferable to use a longer MCL than in dynamic mode; a longer MCL with small spring constant values allows large deflection magnitudes to be achieved [71,73].

Both modes have different strengths and weaknesses, which make them more or less suitable for different tasks. In the dynamic mode where the mass of the adsorbate is known, the total amount of adsorbate on the surface can be estimated [74]. However in the static mode, the absolute amount of molecules adsorbed on the surface is difficult to obtain due to the sufficient lack of knowledge about surface coverage [70,71,74]. The main advantage of the static mode is simplicity, since it does not require any complicated peripheral devices, such as a high-frequency readout setup or an actuation system to excite the MCL [71].

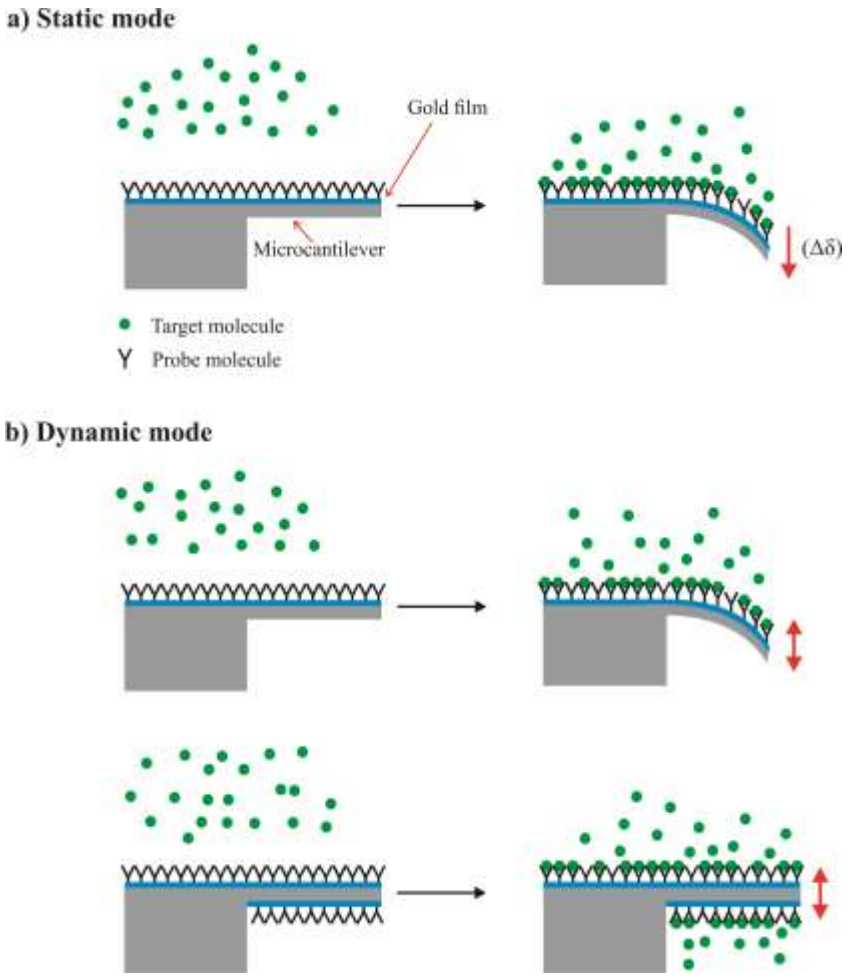

Figure 2.4: An illustration of a side view of the different modes of operation for MCL sensors, where the capture of the target molecules in a) Static mode results in a change in surface stress or b) Dynamic mode results in a change in mass. Adapted from Figure 3.6 in [73].

2.3.3 Static Mode

In the static mode, the interaction between the target molecules and the probe molecules on the MCL surface generates a differential surface stress causing the MCL to deflect [65]

(Figure 2.4a). The OBDS is the most common method used for quantifying MCL deflections. When a laser beam is focused on the apex of the MCL, the laser beam is reflected off the gold coating (Figure 2.5). The reflected laser beam is then detected by a position sensitive photodiode (PSD). As the MCL bends, the position of the reflected laser changes and the displacement on the PSD is then used to determine the deflection [63].

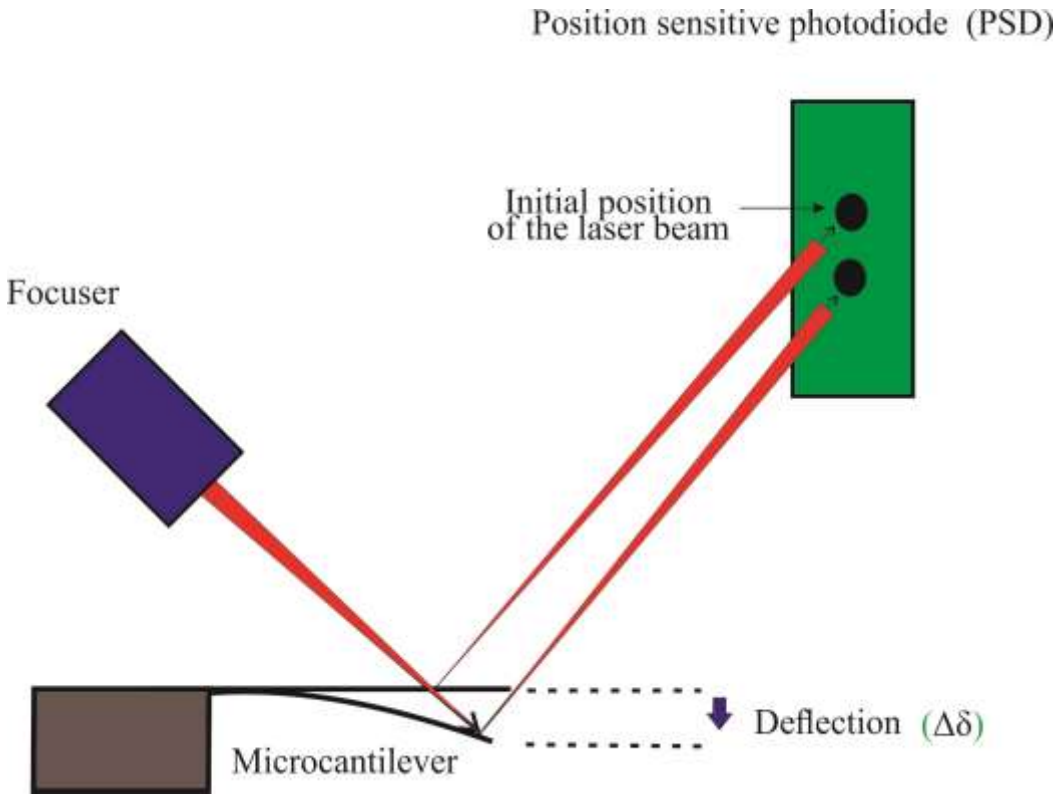

Figure 2.5: A schematic representation of the OBDS. An optical beam is focused on the apex of the MCL. The optical beam reflects off the MCL onto the PSD. As the MCL bends the reflected beam moves to a new position on the PSD.

2.3.4 Dynamic Mode

In the dynamic mode, the resonance frequency of the MCL changes as a result of added mass from the adsorption of target molecules on the MCL surface [73] (Figure 2.4b). Using the dynamic mode, it is possible to associate the change in vibrational frequency to the amount of mass that is adsorbed on the MCL [70,75] using the formula

$$\Delta m = \frac{k}{4\pi^2}\left(\frac{1}{f_0^2} - \frac{1}{f_1^2}\right) \quad (2.1)$$

where Δm is the change in the mass; f_0 and f_1 are the resonance frequencies of the MCL before and after adding the mass, respectively and k is the spring constant of the MCL.

2.3.5 Surface Stress Formation on MCL Sensors

Understanding the surface stress induced during molecular interactions is essential to the study of probe-target interactions, such as detecting heavy metals in water. A detailed understanding of the causes of the variations in the surface stress at the nanoscale level helps researchers develop and improve the accuracy and utility of the data that is collected through these interactions to interpret different surface phenomena. The development and improvement of MCL based sensors and their applications is a result of significant ongoing research [75,76].

There are three main forces that cause a surface stress on MCL surfaces as a result of probe-target interactions: electrostatic interactions; Lennard-Jones interactions; and, charge transfer and surface charge redistribution [77]. Electrostatic interactions are the primary intermolecular forces involved during the interactions between the probe and target molecules [77]. Lennard-Jones interactions are a type of intermolecular force that can be either repulsive (Pauil exclusion) or attractive (van der Waals interactions) [73]. These forces occur between neighboring adsorbed molecules on the MCL surface. Interactions between gold and absorbed atoms can also cause surface stress generation through charge transfer and surface charge redistribution [77]. These causes of surface stress can all contribute to the overall surface stress that is measured.

These three sources differ in how much stress they are able to produce. Electrostatic interactions produce a small amount of surface stress as pointed out by Xie [78] and generally account for less than 10% [75] of surface stress, with the greatest amount of surface stress being generated by the third method of charge transfer and surface charge redistribution [75]. Broniatowski (cited in [79]) explains that Lennard-Jones interactions "at room temperature are negligible for systems such as highly ordered alkanethiol SAMs on Au". Additionally, molecular simulations performed by Godin *et al*. [79] also showed that Lennard-Jones interactions produce relatively small surface stress.

As binding events occur between the functionalized surface of the MCL and the adsorbate molecules, the electronic properties of the gold substrate alter [80,81]. Therefore, the bond strength of the gold surface decreases, causing an increase in the interatomic distance [73,75]. Consequently, both electronic charge densities surrounding the bulk atoms and the surface atoms of the gold layer are disrupted as a result of the transformation of the electronic charges from the gold surface atoms towards the adsorbed molecules [75]. The reconstruction of the surface atoms and the redistribution of the electronic charge on the gold surface have been believed to be the predominant source of induced surface stress in several reaction systems such as alkanethiols [75].

In our case, the surface stress in the following experiments, is produced as a result of the surface stress difference on both sides of the MCL surface. Adsorption of molecules (i.e. Hg, Fe, Pb) on the receptor layer (i.e. calixarene) on the coated surface induces a surface stress different than the opposing surface, thus, a mechanical deflection of the MCL is produced.

2.3.6 Tensile and Compressive Stresses

Tensile stress and compressive stress are the two types of surface stress that can form on a MCL surface.

Compressive stress, which causes a downward bending of the MCL, occurs as a result of repulsive forces between probe molecules on the MCL surface [76,82] (Figure 2.6a). A

tensile stress occurs when the MCL bends upwards and is generated by attractive interactions between molecules being adsorbed on the MCL surface (Figure 2.6b).

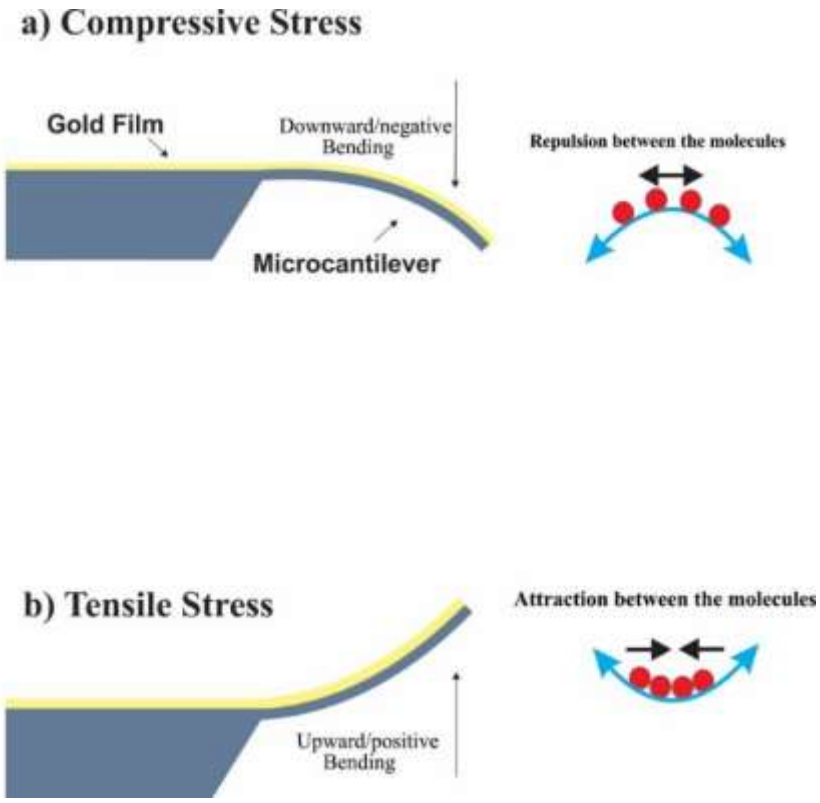

Figure 2.6: An illustration of a MCL bending in response to the formation of surface stress changes on the MCL surface because of a) compressive stress caused by molecular repulsion and b) tensile stress caused by molecular attraction on the functionalized surface.

2.4 Detailed Overview of Calixarenes

The work presented in this thesis is part of an ongoing research partnership between the Physics research group of Dr. Beaulieu and Dr. Georghiou's group in the Department of Chemistry at Memorial University. This interdisciplinary research group investigates the

application of calix[n]arene-functionalized MCL sensors for detecting heavy metals in fresh water.

2.4.1 Calixarenes

C. D. Gutsche first introduces the term calixarene in 1978 to describe the cyclic oligomers formed from the reaction of *p-tert*-butyl phenol and formaldehyde [83]. Calix[*n*]arenes, where *n* is the number of phenolic rings and can be 4, 6 or 8 [83], are macrocyclic compounds that are under intense investigation due to their desirable chemical properties, such as the variation of their cavity sizes and their capacity for being modified [84,85].

Accordingly, calix[4]arene derivatives and their possible applications are of great interest, [83,86]. One of the unique properties of calixarenes is their ability to be functionalized at both rims to suit specific functionalities [1,87] (Figure 2.7). In addition to their ease of preparation, calixarenes have deep cavities and are electron-rich. For this reason, they are able to participate in π-electron interactions with electron-deficient guests. Thus, they have the potential to serve as host molecules [82,88].

Recent research by Dr. Georghiou's group has determined that calix[4]arenes were capable of binding with a gold surface to form a stable self-assembled monolayers (SAM) and to form bonds with distinct metal cations [89,90]. Other research has shown similar findings [91,92], illustrating the great utility of calix[4]arenes with functional groups on the upper and lower rims (Figure 2.7).

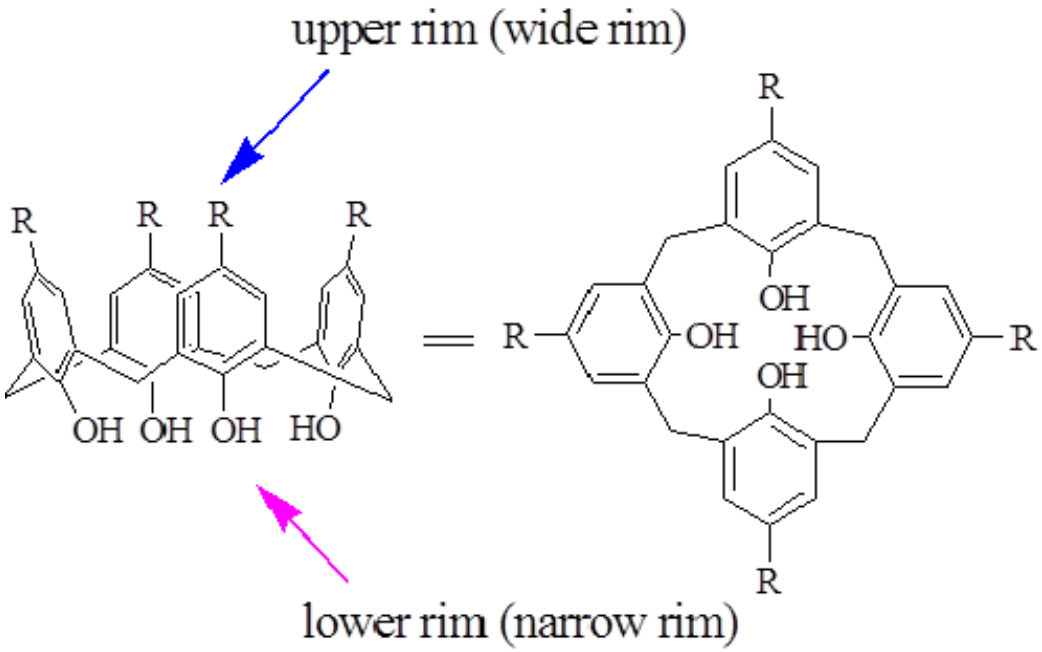

Figure 2.7: Schematic representation of the general structure of calix[4]arene. Calix[4]arene is comprised of two rims, an upper rim and a lower rim. The upper rim has *t*-butyl groups which can be easily modified with any functional group (R) while the lower rim has hydroxyl groups which are less subject to modification. Adapted with permission from Figure 1 in [90].

2.4.2 Three Forms of Calix[4]arine-functionalized Microcantilevers (MCLs)

Three types of calix[4]arenes were synthesised by Dr. Georghiou's group (Figure 2.8) and were investigated as functionalized layers using MCLs by our group.

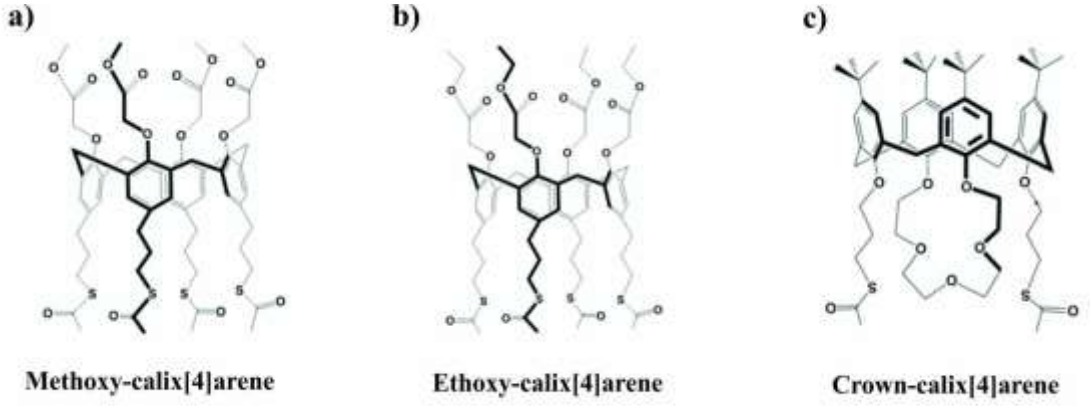

Figure 2.8: Schematic representation of the three different types of calix[4]arenes synthesized by Dr. Georghiou's group. a) methoxy-calix[4]arene, b) ethoxy-calix[4]arene, c) crown-calix[4]arene. Reprinted with permission from Figure 8 in [93].

The results of the work from Alodhayb *et al* using these three types of calix[4]arenes as receptive layers for MCL sensors is particularly relevant to the topic of this dissertation. Their results indicated that all three types of calix[4]arene-functionalized MCLs were capable of detecting trace concentrations of metal ions in aqueous solutions and each type of calix[4]arene was found to be sensitive to different and specific metal ions (Figure 2.9) [89,90,94]. For example, methoxy-calix[4]arene-functionalized MCLs were found to be highly sensitive towards Ca^{2+} ions, whereas crown-calix[4]arene-functionalized MCLs were shown to bind preferentially to Cs^{2+} ions, and ethoxy-calix[4]arene-functionalized MCLs were found to bind almost equally well with both Ca^{2+} and Sr^{2+} [89,90,94].

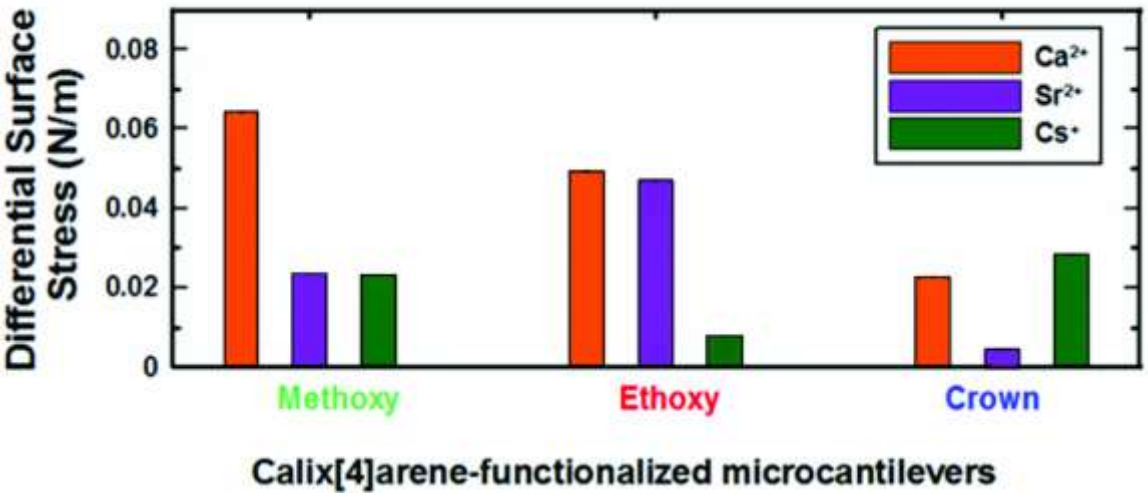

Figure 2.9: Comparison of the deflection of methoxy-calix[4]arene, ethoxy-calix[4]arene, and crown-calixarene functionalized cantilevers from Ca^{2+}, Cs^{2+}, and Sr^{2+}. Reprinted with permission from Figure 8 in [93].

2.4.3 Synthesis of a New Anthracenyl-triazolyl Bimodal Calix[4]arene

A fourth calix[4]arene was synthesized by Dr. Georghiou's group at Memorial University, namely the anthracenyl-triazolyl functionalized bimodal calix[4]arene. The functionalization of triazole-calix[4]arene involves the modification of its upper and lower rims. The triazole-calix[4]arene self-assembles to form a monolayer on the gold surface as a result of Au-S bonding (Figure 2.10). The formation of the SAM can be accomplished by immersing gold coated MCLs into a solution of triazole-calix[4]arene for 2h at room temperature. The binding capabilities of the newly synthesized triazole-calix[4]arene towards $Hg^{2+,}$ Fe^{3+}, Ni^{2+}, Zn^{2+} and Pb^{2+} in aqueous solutions were investigated during the course of this work.

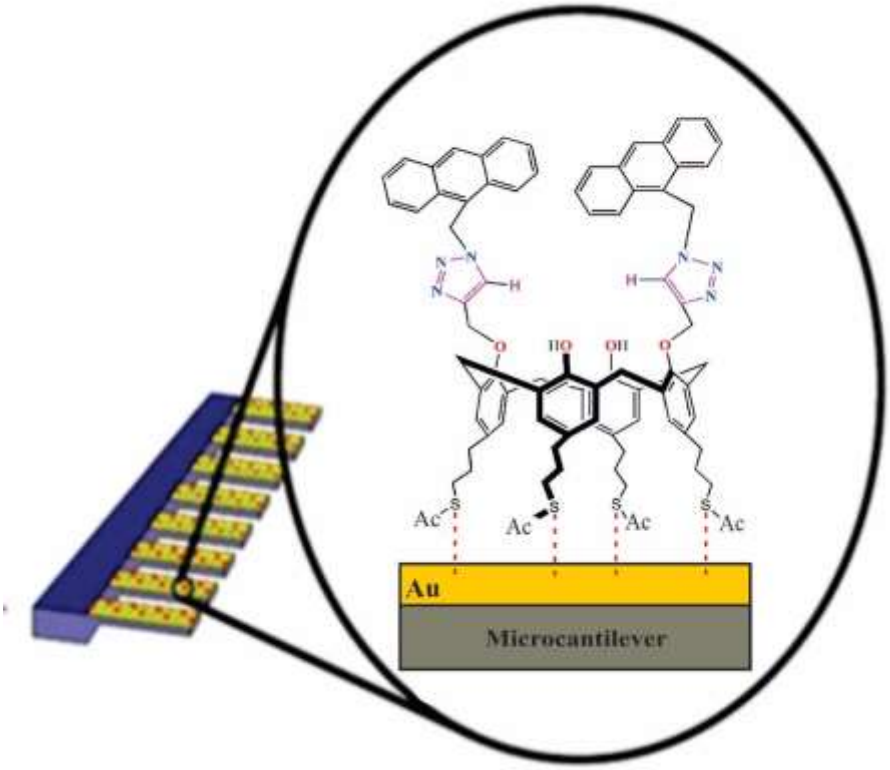

Figure 2.10: A schematic diagram of the triazole-calix[4]arene immobilization on a gold coated MCL surface forming a stable SAM) due to the polar Au^{+} S^{-} bonding. Reproduced with permission from Figure 2 in [1].

Numerous physical and electrochemical techniques can be used to characterized the surface structure of SAMs, such as scanning probe microscopy techniques (i.e. AFM [95] and STM [90]), X-ray diffraction [96], optical ellipsometry [97], contact angle measurements [98], and cyclic voltammetry technique [99]. The use of AFM and STM was used to determine the high order of the SAM of different types of calix[4]arenes. While STM was capable to characterize some types of calix[4]arene (i.e Ethoxy-calix[4]arene [90] and Crown-calix[4]arene [94]), we were not able to obtain quality images of triazole-calix[4]arenes.

2.5 Attempts to Characterize the Formation of SAM of Triazole-Calix[4]arene Using AFM

Tapping mode AFM was used to study the topography of immobilized triazole-calix[4]arene on gold films. A 40 nm gold film deposited on a mica substrate was thermally annealed at 275°C for a week to decrease the roughness of the surface [100]. Following the annealing process, the Au-substrate was incubated for 2h in a 1:9 dichloromethane:ethanol solution of triazole-calix[4]arene (~2.0×10^{-5} M) and then imaged by AFM. Despite several attempts, it was not possible to characterize the triazole-calix[4]arene molecules. Difficulties in obtaining molecular-resolution images could be attributed to the floppy end group on the lower rim of the triazole-calix[4]arene. Such difficulties prevented AFM imaging from acquiring clear images and resulted in blurred images.

Chapter 3 Methodology

3.1 Microcantilever (MCL) Surface Functionalization

In order to transform a MCL for performing static deflection sensing, one side of the cantilever needs to be coated with molecules made to react with a target analyte [77]. In this work, functionalizing the MCL was performed using the following procedures:

a) MCL cleaning using acid based methods.

b) Thin film deposition using sputter deposition.

c) Immersing of the coated MCL into a solution containing molecules of interest, so that a self-assembled monolayer (SAM) can be formed.

3.1.1 Microcantilever (MCL) Cleaning

The presence of contaminates such as organic and inorganic particulates has a significant impact on the surface properties of MCLs and in particular on molecular absorption [73]. In this work, the Radio Corporation of America (RCA) and Piranha cleaning methods, as described below, were used to clean the MCL surface.

The RCA Cleaning Method

The RCA cleaning method was used to remove organic residues, the oxide layer, and ionic contaminants from the silicon MCL surface. It was performed by the following three steps.

Step 1: SC-1 (Standard Clean)

The SC-1 solution was used to remove any traces of organic residues. In the first step, an alkaline solution was prepared by mixing deionized water (DIW), aqueous ammonium hydroxide (NH_4OH), and aqueous hydrogen peroxide (H_2O_2) in a ratio of 5:1:1, by volume. The solution was heated to 70-80°C and then the MCL was immersed for 10 minutes and then rinsed with DIW for 3 minutes.

Step 2: Hydrofluoric Acid (HF) Solution

This step removes the native oxide layer on the surface of the silicon MCL. In this step, the MCL was dipped into a 2% HF solution for 2 minutes and then rinsed with DIW for 30 seconds. The HF solution is a mixture of HF and DIW in a ratio of 1:50, by volume.

Step 3: SC-2 (Standard Clean)

The SC-2 clean solution dissolves ionic contaminations, residual trace metals, and inorganic residues. The SC-2 solution consists of a mixture of DIW, hydrogen chloride (HCl), and hydrogen peroxide (H_2O_2) in a ratio of 6:1:1, by volume. This solution was heated to 80°C and the MCL was placed into the solution for 15 minutes and then rinsed with DIW for 5 minutes.

The Piranha Cleaning Method

The next step in the cleaning treatment of MCLs was the use of the Piranha cleaning method, which was performed immediately prior to the functionalization of the MCL surface. The Piranha solution is a mixture of hydrogen peroxide (H_2O_2) and sulfuric acid (H_2SO_4) in a ratio of 1:3, by volume. The MCL was immersed in a Piranha solution for 10 minutes followed by rinsing twice in ethanol and DIW. The MCL was then dried in an oven for 5 minutes at 275°C.

3.1.2 Thin Film Deposition

The deposition of a thin metallic film can be accomplished using a variety of techniques, such as thermal evaporation and sputter deposition [101]. In the first method, a thin film of the material of interest is condensed onto a substrate by means of a heated source; however, the latter method was used in this work and is described in detail below.

In this work, sputter deposition was used to deposit a thin gold film on the silicon MCL. Gold is widely used to attach sensing molecules because it does not easily oxidize [102]. Sputter deposition has many advantages over other deposition techniques, including the possibility of depositing a variety of materials and the ability to control various sputtering parameters, such as gas flow and deposition rate [103].

A sputtering system consists of a vacuum chamber, a target material, a magnetron, and a high voltage power supply (Figure 3.1).

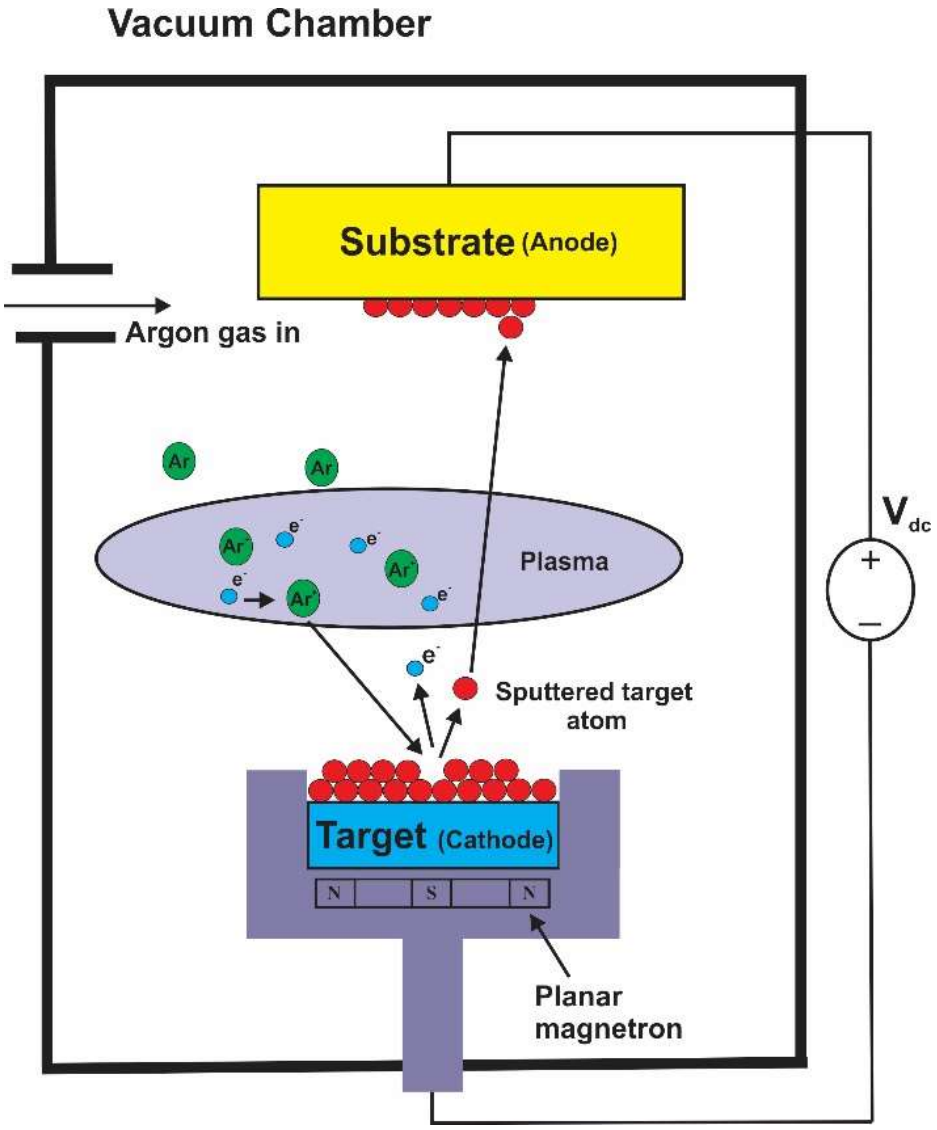

Figure 3.1: A schematic representation outlining the functions of a sputter deposition system. In this system, argon gas is ionized by an applied electric field between an anode and a cathode. These ionized Ar ions collide with the target and eject target atoms, which in turn get deposited on the substrate, forming a thin film.

Sputter deposition of a thin film is conducted by first evacuating the chamber to 10^{-6} Torr after which argon gas is introduced into the chamber. An applied voltage between the target material (cathode) and the substrate (anode) produces an electric field. This field ionizes the Ar gas, resulting in the generation of a plasma. Magnets placed behind the target create a magnetic field that traps electrons near the target and causes them to travel on a spiral trajectory and strike Ar atoms. This increases the ionization of Ar atoms, which leads to an increased deposition rate. Energetic Ar^+ ions bombard the surface atoms of the target with sufficient kinetic energy to expel target atoms. The target atoms are ejected from the source and condense on the substrate creating a thin film.

In this work, a sputter coater[2] was used to deposit a 5 nm layer of Inconel (0.8 Ni:0.2 Cr) directly on the substrate at a power of 40W and a rate of 0.3 Å/s for 2 min and 50 sec. This thin film serves as an adhesive layer between the Si substrate and the Au film. Afterward, a 40 nm gold film was deposited, at a power of 10W and a rate of 0.2 Å/s for 33 min and 20 sec.

3.1.3 Functionalization Procedure of MCL Array

Initially the MCL arrays were functionalized using a simple beaker method. This was a straightforward procedure where the MCL array was placed in a beaker and immersed in a solution with the probe molecules of interest. The formation of the SAM on the MCL surface requires the gold coated MCL surface to be in contact with the solution of probe

[2] Corona Vacuum Coaters, Vancouver, BC

molecules for an extended period of time so that the molecules can interact. Since the length of incubation time impacts the formation of the sensing layer [103], in preparation for this research a variety of incubation times for triazole-calix[4]arene were tested. Based on the criteria of equilibrium state and deflection magnitude, the best SAMs were formed in 2h. Thus, we used a 2h incubation time at room temperature consistently for all the following experiments.

3.2 Experimental Set Up for 16 MCLs

Two members of our research group, Alodhayb and Rahman, recently developed an experimental system [93] that was well suited to our current research.[3] The experimental set up used in this work consists of five major parts (Figure 3.2).

1) A fluid cell within which the MCL arrays were mounted.
2) The fluid delivery system consisting of polyether ether ketone (PEEK) tubes used for the transportation of fluid in and out the fluid cell.
3) An optical microscope situated over the fluid cell.
4) Optical focusers and a 2D-position sensitive detector (PSD) used to monitor the MCL deflection.
5) A motorized translation stage.

[3] A detailed description of the working principle of this system can be found in [93]

The experimental set up was mounted on a vibration isolation platform to increase the stability and to reduce the effects of mechanical vibrations and surrounding noise from the environment.

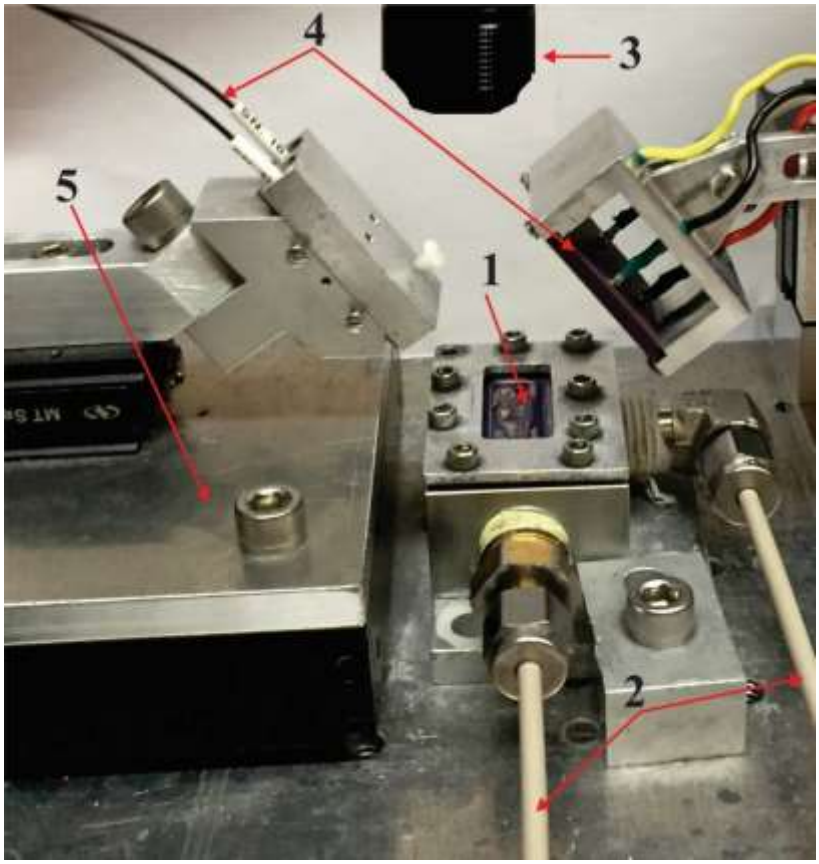

Figure 3.2: A photograph of the 16 MCL sensor setup. The main parts of this system are 1) Fluid cell, 2) Fluid delivery system consists of two PEEK tubes, 3) Optical microscope, 4) 2D-PSD and optical focusers held by an arm attached to a translation stage, and 5) Translation actuator stage assembly.

After the MCLs were functionalized, they were placed into an experimental set up for subsequent use. Item 1 in Figure 3.2 is the fluid cell, which is designed to accommodate two 8 MCL arrays. The two PEEK tubes (item 2) attached to the fluid cell were used to carry the solution to and from the cell. The solution was introduced to the fluid cell through the input tube using a programmable syringe pump (not pictured in figure 3.2). Item 3 is a camera that allows greater visibility to ensure that the laser was positioned correctly on the MCLs. Part 4 shows the two optical focusers, which were used to adjust the position of the laser beam generated from the laser diode. Part 4 also shows the two axis PSD[4] that was used to detect the laser beam reflected off the MCLs. The PSD was adjusted so that the laser beam reflecting off each MCL surface hits the active area of the device. The optical focusers were mounted on an arm, (item 5), which allows an actuated translation stage[5] to move the optical focusers back and forth so that the laser beam can strike all 16 MCLs.

3.2.1 The Fluid Cell and Fluid Delivery System

All experiments were conducted in a stainless steel fluid cell that is corrosion resistant and known to not react with the reagents used in this work. This is important to minimize the effect of the fluid cell on the experimental results, thus increasing the accuracy of the measurements.

---

[4] 2L10SP, On-Trak Photonics, USA

[5] Thorlabs Inc, USA

The fluid cell is composed of four major parts (Figure 3.3) and was located at the center of the platform that holds the experimental set up. It has two slots where the active and the reference MCL arrays (1) were mounted and held by stainless steel spring clips (4). The solution containing the analyte entered the cell at the inlet hole (2) and then exited through the hole (3) (Figure 3.3).

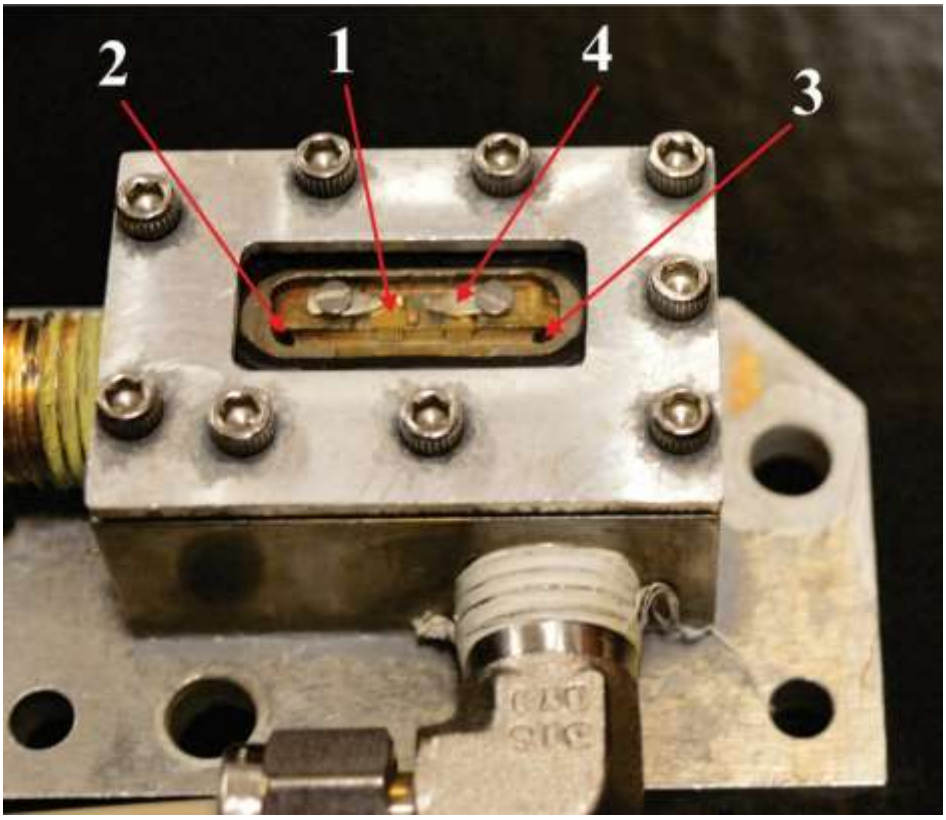

Figure 3.3: A photograph of the fluid cell used in this work. The main components of cell are 1) 8 MCL array; 2) an inlet hole for the solution to enter the fluid cell; 3) an outlet hole for the solution to exist the fluid cell; and, 4) a spring clip used to hold the MCL array in the slots.

In order to seal the cell, a Viton® O-ring was used to seal it with a specially treated, anti-reflective glass.[6] This was done to eliminate the reflection of the optical beam from the glass/air and the glass/liquid interfaces which were found to affect the PSD measurement.

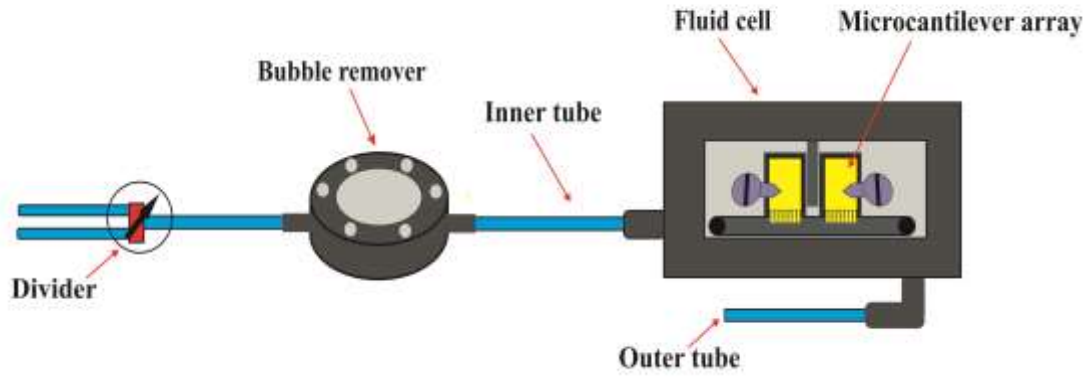

Figure 3.4: A schematic depiction of the fluid delivery setup used to bring target solutions to the cell. A divider is used to select which inlet tube will supply fluid to the cell. The bubble remover is used to prevent bubbles from entering the cell.

A divider was used to switch between syringes to allow different solutions to enter the cell. Unfortunately changing the syringes often led to the formation of bubbles inside the fluid cell. The presence of bubbles inside the fluid cell can interfere with the deflection of the MCLs and thus ruin the experiment. A bubble remover, designed by Dr. Beaulieu, was used to prevent bubbles from entering the fluid cell [93].

[6] ASE Optics, USA

The bubble remover is composed of a cylindrical cavity with one inlet and one outlet for the liquid (Figure 3.5). The inside of the cavity is separated into two parts by a stainless steel divider with 1 mm holes and is sealed with a glass disk and an O-ring at the top. As a second measure of prevention, a fine mesh was placed on the inlet side in front of the 1 mm holes to ensure that no bubbles made their way to the outlet side.

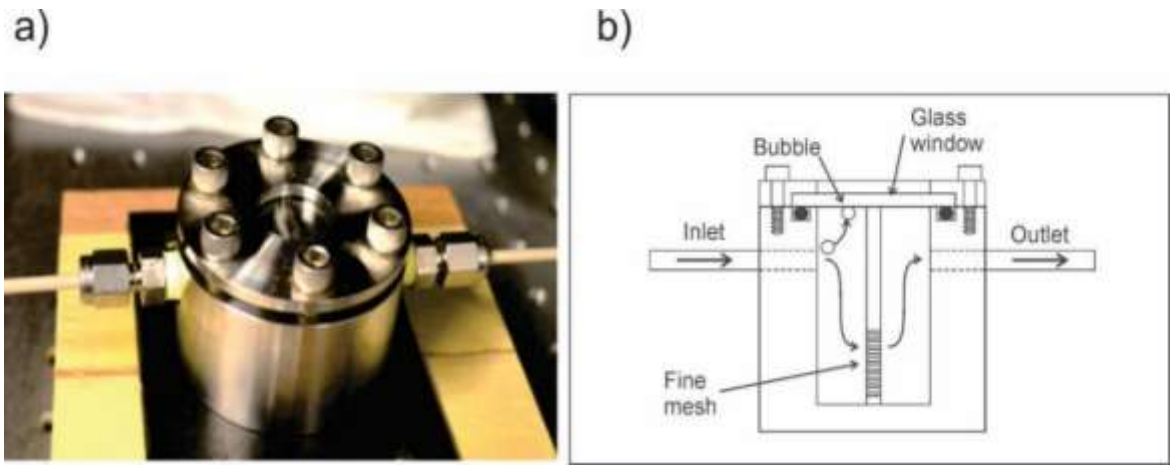

Figure 3.5: a) A photograph and b) a schematic depiction of the bubble remover. Reprinted with permission from [93].

3.2.2 Optical Microscope

An optical microscope was used to visualize the position of the optical beam on the MCLs (see Figure 3.6). This camera was placed directly above the fluid cell, as previously illustrated in part 3 of Figure 3.1.

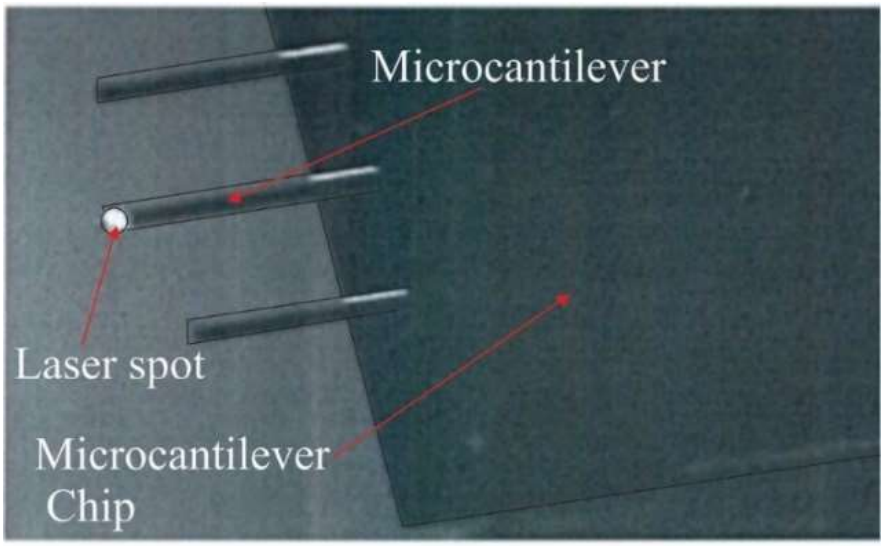

Figure 3.6: A photograph of the spot produced on the tip of the MCL by the laser beam. The use of the optical microscope facilitates adjusting the position of the laser beam on the MCLs.

3.2.3 Lasing System and PSD

In this work, a 17 mW laser diode[7] was used to emit a laser beam at a wavelength of 635 nm. The diode was mounted on a laser diode mount[8] and powered by a precision current source.[9] The temperature of the laser diode was controlled by a precision temperature controller.[10]

---

[7] ADL-63153 TL, OZ Optics LTD

[8] LDM-4980

[9] LDX-3412, ILX Lightwave Corp

[10] LDT-5412, ILX Lightwave Corp

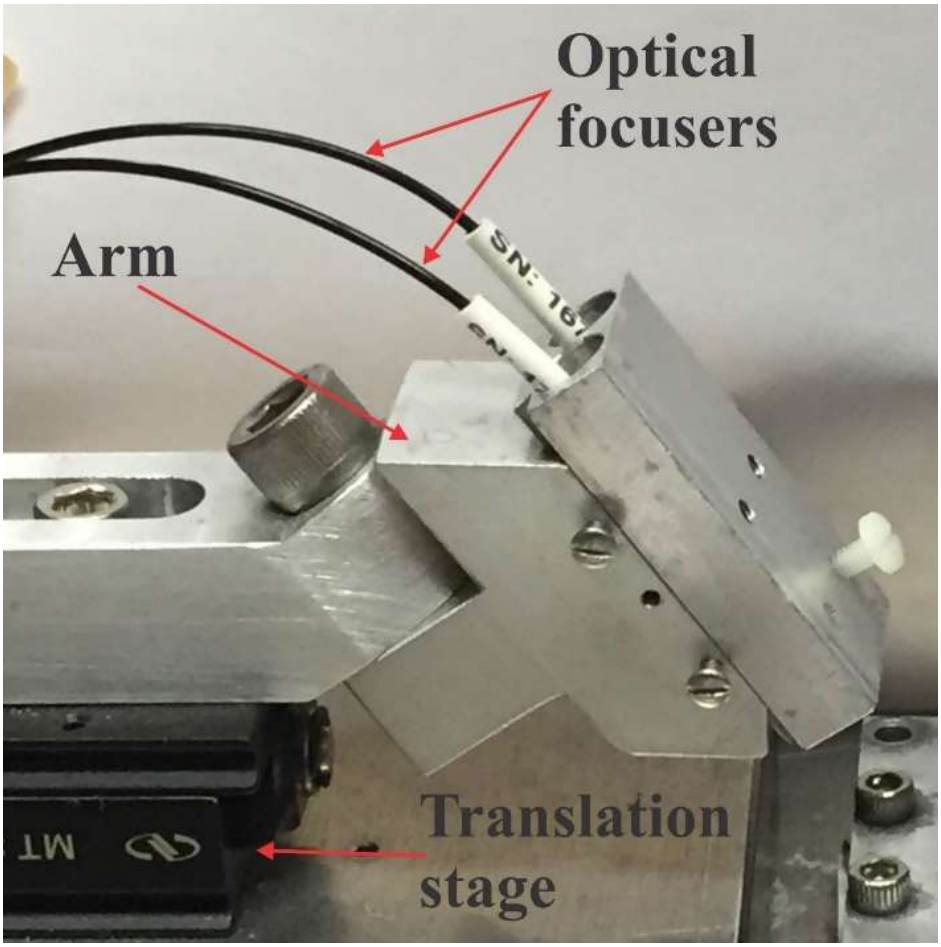

Figure 3.7: A photograph of the optical focusers held by an arm and mounted on an actuated translation stage.

Two optical focusers[11] were held on a pivoting arm allowing more control of the laser spot position on the MCL apex (Figure 3.7). The arm, in turn, was mounted on an actuated translation stage, allowing the laser beam to scan over all 16 MCLs.

[11] LPF-01-635-4/125-S-2.6-15-4.5AC-40-3S-1-1-SP, OZ Optics

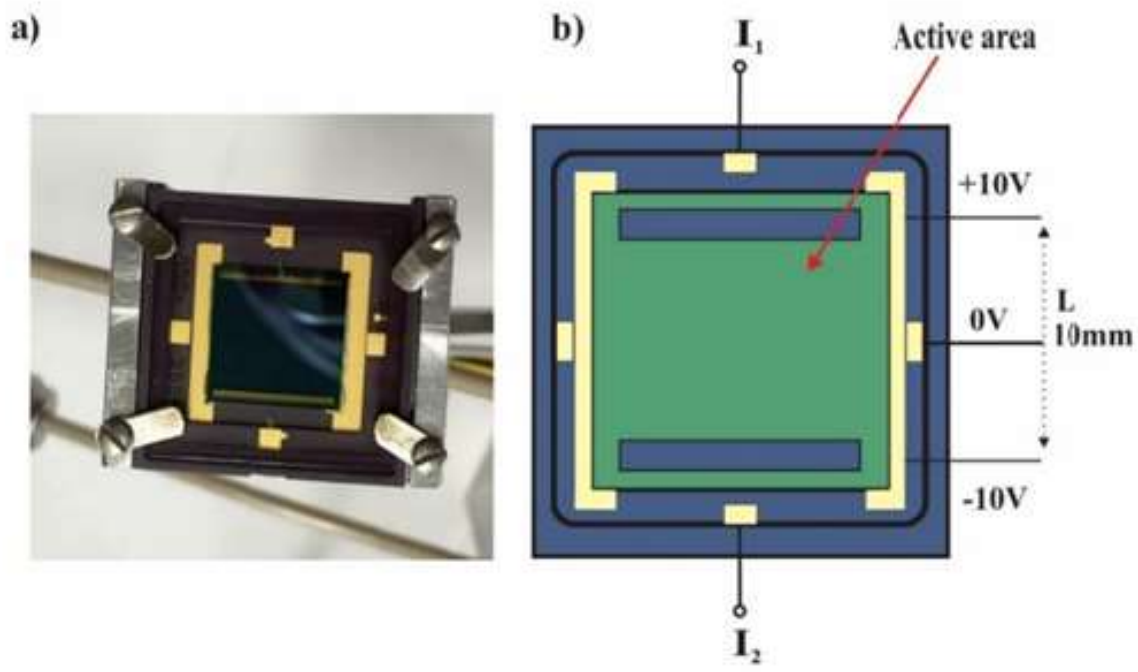

Figure 3.8: A a) photograph and b) schematic illustration of the 2D-PSD. The 2D-PSDdetects when the laser beam hits the active area using two photocurrents, I_1 and I_2.

A PSD detects the reflected laser beam and converts this into a recordable electrical signal. The position of the beam on the PSD surface is linearly related to the PSD voltage. The output voltage of the PSD changes as the position of the incident beam shifts on the PSD due to the MCL deflection. The PSD has an active area of 10 × 10 mm, where the center of this area corresponds to an output voltage of 0 V (Figure 3.8b). When the beam shifts upwards to the top at +5 mm, the voltage increases to +10 V, and deceases to –10 V when the beam moves downwards to the bottom of the active area. When the laser beam strikes the active area of the PSD, two photocurrents, I_1 and I_2, are generated and converted into a

voltage signal through an amplifier. The amplified voltages are interpreted through a data acquisition (DAQ) card.

3.2.4 The OBDS

The OBDS is a simple, reliable, and commonly used technique for monitoring the MCL's deflection [104]. The OBDS, which is also used in AFM systems, consists of three main components: a laser beam, a MCL, and a PSD. When the MCL bends, the incident laser beam reflects from its surface changing its position on the PSD. The change in the displacement of the laser beam on the PSD surface can then be used to determine the MCL response.

Beaulieu *et al*. [63] have developed a mathematical model to relate the MCL bending to the signal of the PSD. They stated that the OBDS can be completely characterized using geometric optics. The OBDS can be characterized by determining the following values: θ, φ, ζ, L, D, and CL, where θ represents the angle of inclination of the laser beam, φ is the azimuthal angle, ζ is the PSD angle with respect to the *x*-*y* plane, and D is the distance between the incident beam and the base of the MCL (Figure 3.9). The PSD is located at a distance L from the incident beam on the MCL's apex and CL represents the MCL length.

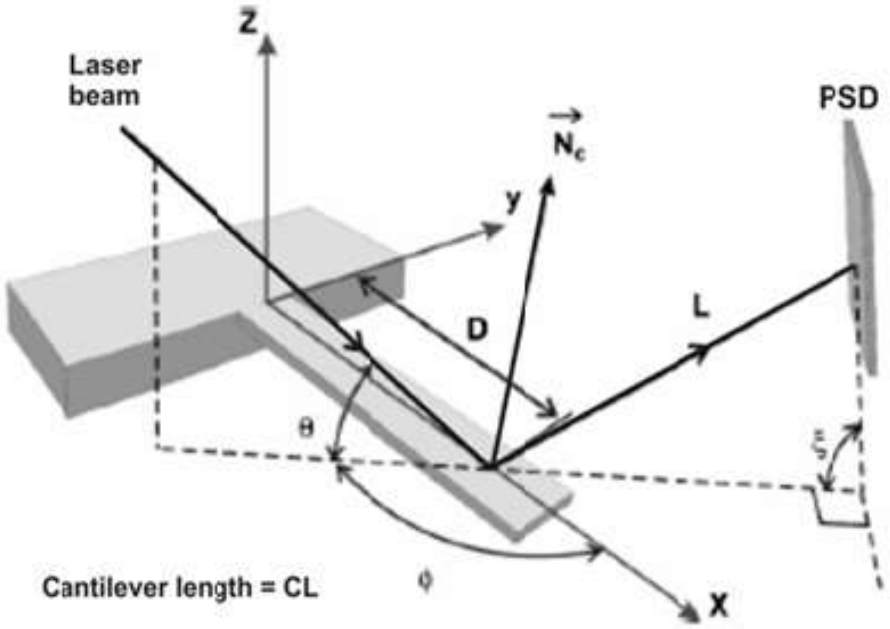

Figure 3.9: A schematic representation of the OBDS illustrating how the deflection of the MCL and the PSD signal can be interpreted by considering simple geometric optics. Reproduced with permission from Figure 1 in [58].

3.3 Delimitations

In this original research, we limit our investigation to the interaction between the triazole-calix[4]arene functionalized MCLs and five metal ions. We examined lead, mercury, nickel, iron, and zinc, chosen from the Canadian Environmental Quality Guidelines. We limited our analysis to five elements to keep the size and scope of our current research manageable within the given timeline. We were most interested in determining mercury

interactions with the triazole-calix[4]arene functionalized MCLs, and the other four were included for comparison.

3.4 Experimental Procedures

In this study, we analyzed the effects of triazole-calix[4]arene used as functionalized layers for cantilever sensors. The gold coated MCLs were functionalized by submerging them in a prepared solution of 1:9 dichloromethane:ethanol solution of anthracenyl-triazolyl functionalized bimodal calix[4]arene (~2.0×10^{-5} M) for 2h. This immersion allowed a SAM of the calix[4]arene to form on the gold surface. At the same time, the reference MCLs were prepared by incubating them for 2h in a 1.0 μM solution of decanethiol. The MCLs, in both cases, were put into a standard glass beaker to incubate. This first step functionalizes both sets of MCL arrays with the proper sensing layers for our experiments using the active and reference MCLs.[12] Following this, the MCLs were transferred from the beaker into a flow-through cell and sealed.

Once the cell was closed, research-grade DIW[13] was introduced from the first syringe at a flow rate of 0.1 ml/min until thermal equilibrium was achieved. This point was determined by monitoring the MCL's deflection signal until no changes were observed. This step was important since we cannot accurately measure the deflection of the MCLs unless thermal

[12] While this is a straightforward procedure it limits our ability to functionalize the MCLs individually, in order to test multiple sensing layers at the same time. Our solution to this problem will be discussed in Part II.

[13] UltraPure™ DNase/RNase-Free Distilled Water, Thermo Fisher Scientific Inc

equilibrium was reached as a baseline. The aqueous solution containing the target ions was then introduced to the MCL arrays contained within the fluid cell at a constant flow using the second syringe. The MCLs then began to deflect as a result of the complex interactions between the sensing layer and the target ions.

This aforementioned process was performed in each experiment, and the difference between the experiments was just the target solutions. The target solutions varied in either the target ions being observed or the concentration of the target ions. In each experiment, the deflection of the MCLs was recorded using an OBDS.

3.5 The Motion of Target Ions in the MCL Fluid Cell

In this work, the same methodology was used for all experiments. At the beginning of each experiment, the fluid cell was filled with DIW until thermal equilibrium was achieved at which point the target solution was injected into the fluid cell. Because the movement of the solution through our MCL sensor setup is highly laminar as shown by our previous calculations [105], we suspect that there is very little mixing of the target solution with the DIW originally in the cell and that the MCLs are subjected to the full concentration of the analyte within a few minutes.

Chapter 4 Data Analysis and Results

4.1 The Reaction of Triazole-Calix[4]arene Functionalized MCLs with $Hg(ClO_4)_2$

The initial experiments comparing triazole-calix[4]arene functionalized MCLs with reference MCLs were conducted to understand the potential of this new sensing layer. In particular, we investigated the sensitivity of triazole-calix[4]arene functionalized MCLs towards Hg^{2+} ions. The active and reference MCLs were both exposed to an aqueous solution of Hg^{2+} and the deflection was recorded and compared. This section provides a thorough discussion of our results.

In our first experiment, a 2×10^{-5} M aqueous solution of $Hg(ClO_4)_2$ was introduced into the fluid cell that contains two MCL arrays, one active and the other for reference. Using an array of each type yields results consistent with experiments performed many times while guaranteeing exact same experimental conditions. The deflections of both arrays of MCLs are presented together for comparison in Figure 4.1.

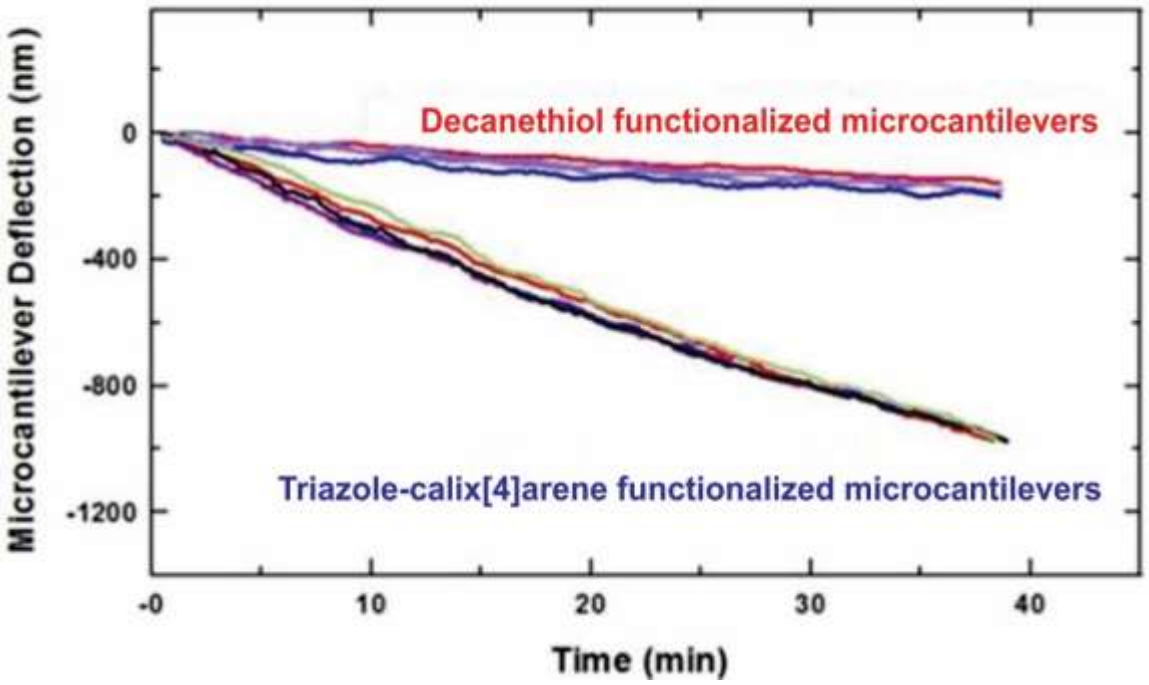

Figure 4.1: Microcantilever deflection versus time for active and reference MCLs exposed to a 2×10^{-5} M aqueous solution of $Hg(ClO_4)_2$.

The results illustrated at the top of figure 4.1 are from the reference array, which were functionalized with decanethiols. The curves are very similar, close together, and overlapping, which indicates the high reproducibility and high accuracy of these results. Similarly, the curves from the triazole-calix[4]arene functionalized MCLs are very close together and overlapping, which again suggests that the active MCLs were as reliable as the reference MCLs.

As outlined in detail in the literature review, microcantilever deflections are produced by the formation of a surface stress on the MCL surface as a result of the interaction between

the sensing layer and the target ions (section 2.3.5). In this work the reference MCLs do not have a coating that interacts with the ions, while the active MCLs functionalized with the triazole-calix[4]arene sensing layer were able to capture target ions from the aqueous solution. The reference MCLs have little deflection compared to the active MCLs, but some deflection was expected.

Some of the minor deflection observed can be attributed to nonspecific interactions as well as temperature variation. The second cause of the deflection could result from the absorption of Hg ions in the areas where the Au film was not completely covered by the decanethiol SAM. Incomplete decanethiols SAMs have been observed by other researchers and was not an unexpected factor [106]. The interaction of Hg and Au can cause some deflection as observed by Xu *et al.* in their work with MCL sensors [107]. In order to isolate the deflection caused only by the interactions of the target ion with the sensing layer, the deflection of the reference MCLs was subtracted from the deflection of the active MCLs. The result was the differential deflection signal shown in Figure 4.2.

4.1.1 The Effect of the Concentration Variation on the MCLs Deflection

We investigated the sensitivity of triazole-calix[4]arene towards different concentrations of Hg^{2+}. As discussed in the literature review, the Canadian environmental quality guidelines recommended safe limit for the presence of mercury in water sources in Canada is 0.026 μg/L [39] (section 2.1.5). This value corresponds to a concentration of 1.30×10^{-8} M. The

different concentrations of mercury in aqueous solutions investigated in this section are presented in Table 4.1 and the results are shown in Figure 4.2.

Table 4.1: Results of different concentrations of Hg^{2+} including average deflection at 35 mins, standard deviation, and the Canadian environmental quality guidelines for mercury, presented in equivalent units

Original Units of the Hg^{2+} Solution	**Equivalent Units $\times 10^{-8}$ M**	**Average MCL Deflection (nm)**	**Standard Deviation (nm)**
2×10^{-11} M	0.002	220	14.3
0.026 µg/L	1.30	N/A	N/A
2×10^{-8} M	2	396	18.8
2×10^{-5} M	2000	644	15.7

These results demonstrate that larger deflections were observed for higher concentrations of Hg^{2+}. The results shown in Figure 4.2 for three different concentrations of Hg^{2+} represent the differential measurement (active signal–reference signal) of the MCLs in the array. The inset shows the average MCL deflection at 35 minutes obtained from the three concentrations of Hg^{2+}. Increases in the deflection magnitude of the MCLs was therefore proportional to increases in the concentration of ions in the target solution, which indicates that the sensing layer was interacting with a larger number of Hg^{2+} ions on the MCL surface.

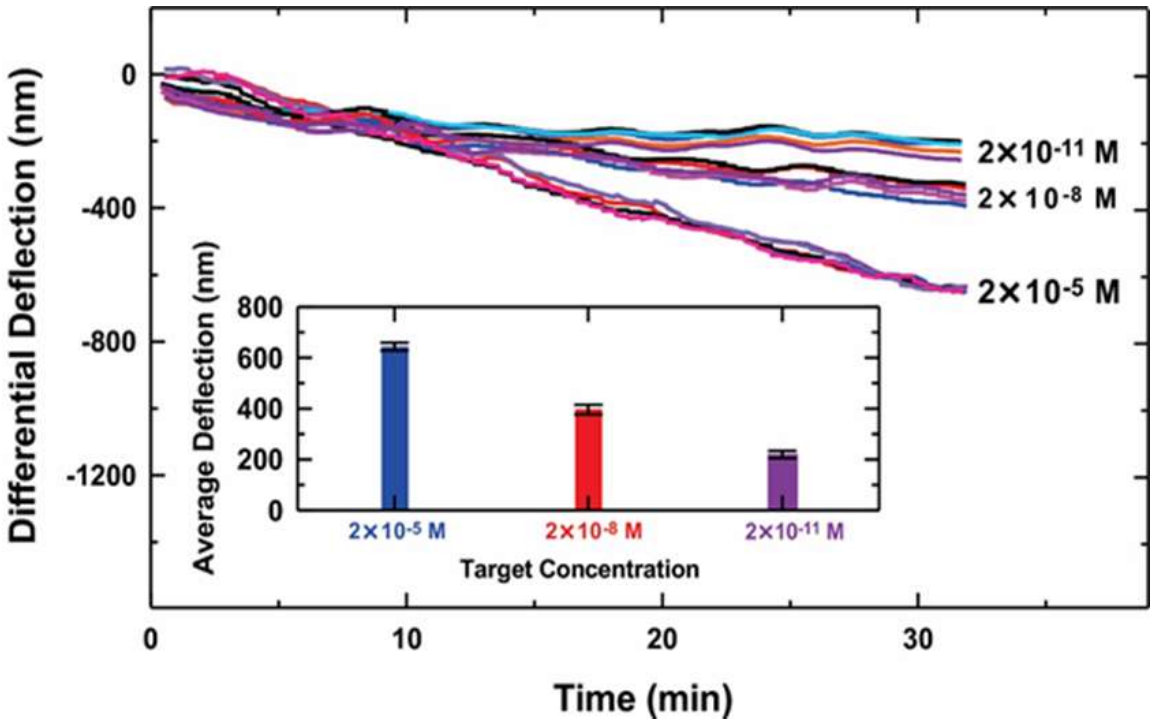

Figure 4.2: Differential deflection versus time for three different concentrations of mercury. The error bars in the inset bar graph indicate the standard deviation between each set of MCLs exposed to the same concentration for three different experiments.

Ultimately, the results indicate that MCL arrays functionalized with triazole-calix[4]arene were capable of detecting trace concentrations of Hg^{2+} ions as low as 10^{-11} M. Moreover, even at such low concentrations, the range of deflections observed were within the range of 180nm to 220nm (Table 4.1). This range of values is still large indicating that triazole-calix[4]arene functionalized MCLs would be able to detect even lower concentrations.

4.2 The Effect of the Presence of Pb^{2+} Ions on the Sensitivity of the Triazole-Calix[4]arene Functionalized MCLs Towards Hg^{2+}

After determining that triazole-calix[4]arene functionalized MCLs are highly sensitive to Hg^{2+} ions, we examine how the presence of Pb^{2+} ions might impact the sensitivity of the triazole-calix[4]arene towards Hg^{2+} ions. We consider three different ways of examining the potential effects of the presence of Pb^{2+} ions in the Hg^{2+} target solution. In the first case, we introduced a solution containing Pb^{2+} ions to the MCL arrays before introducing a solution containing Hg^{2+} ions. In the subsequent experiment, we introduced a mixture of both Pb^{2+} and Hg^{2+} ions at the same concentration in a single solution to the MCL arrays at the same time, and lastly, we introduced a mixture of both Pb^{2+} and Hg^{2+} ions at varying concentrations in a single solution to the MCL arrays at the same time. The results of these experiments are discussed in greater details at the end of this section.

4.2.1 $Pb(ClO_4)_2$ Followed by $Hg(ClO_4)_2$

In this experiment, we aimed to investigate the effect of introducing a 2×10^{-5} M solution of Pb^{2+} followed by a 2×10^{-5} M solution of Hg^{2+} on the sensitivity of triazole-calix[4]arene functionalized MCLs. As before the cell was cleaned and both active and reference MCLs were placed in the fluid cell and then exposed to a constant flow of DIW. As the system reached thermal equilibrium, a 2×10^{-5} M solution of Pb^{2+} was introduced into the fluid cell while the MCL arrays were monitored for 27 mins. After this time a 2×10^{-5} M solution of Hg^{2+} was introduced and the MCLs were again monitored for 27 mins. The results of this experiment are shown in Figure 4.3.

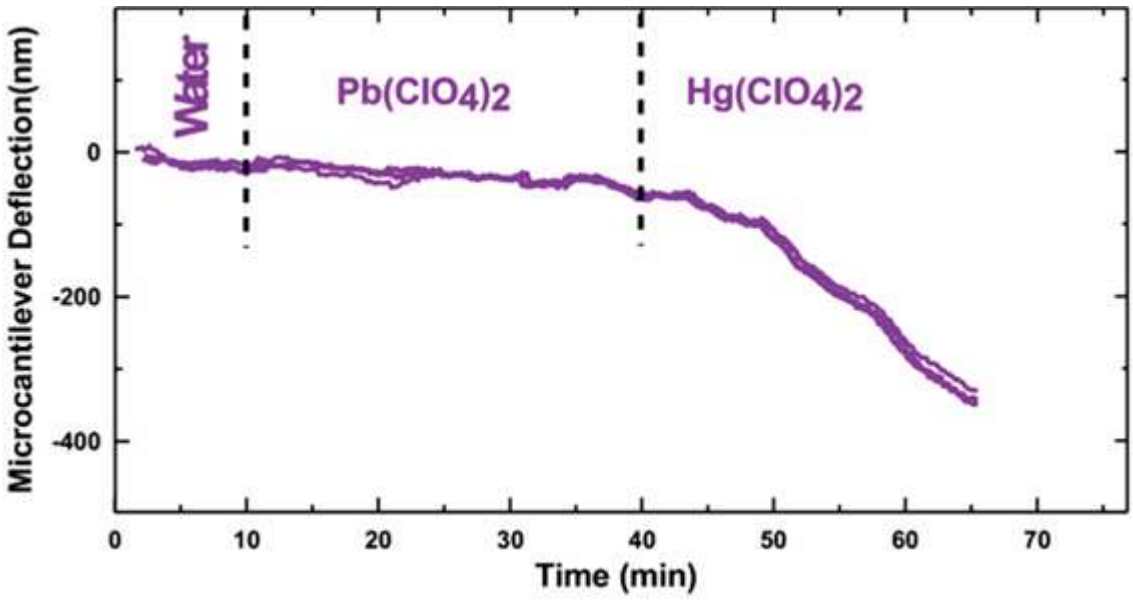

Figure 4.3: Differential deflection versus time for DIW/ $Pb(ClO_4)_2$/ $Hg(ClO_4)_2$ solution.

Introducing $Pb(ClO_4)_2$ into the cell caused the active MCLs to undergo a small deflection indicating that Pb^{2+} ions bonded with the sensing layer (see Figure 2.4a for a visualization of this process). When the 2×10^{-5} M solution of $Hg(ClO_4)_2$ was subsequently introduced into the fluid cell, the triazole-calix[4]arene functionalized MCLs deflected further downwards as expected.

In order to gain more insight into the results demonstrated in Figure 4.3, it was necessary to conduct more experiments with different concentrations of $Pb(ClO_4)_2$ and $Hg(ClO_4)_2$. These experiments are discussed below.

4.2.2 $Hg(ClO_4)_2$ and $Pb(ClO_4)_2$ at 1:1 Introduced at The Same Time

In the second experiment, Pb^{2+} and Hg^{2+} ions were both introduced to the fluid cell in a 2×10^{-5} M solution at the same time with a 1:1 ratio between the two different types of metal ions, and then monitored for 35 minutes. The main objective of conducting this experiment was to see if the combination of the two ions would affect the response of triazole-calix[4]arene functionalized MCLs. The results of this experiment are presented in Figure 4.4 by the blue curve. In this experiment, 50% of the ions in the solution were Pb^{2+} ions and 50% were Hg^{2+} ions, but the concentration of the solution remains 2×10^{-5} M. The deflection magnitude has significantly decreased compared to the case where the two ions were introduced sequentially. This result cannot be immediately explained and thus an experiment including the use of different concentrations (see section 4.2.3) of the two ions was conducted to provide a better understanding of this result.

4.2.3 Hg(ClO4)2 and Pb(ClO4)2 at 1:3 Introduced at the Same Time

In this experiment, 75% of the ions in the 2×10^{-5} M solution were Hg^{2+} and 25% of the ions in the solution were Pb^{2+}. When the equilibrium state was reached, both of the Pb^{2+} and Hg^{2+} ions were introduced to the fluid cell as a single solution and then monitored for 35 minutes. The results of this experiment, represented by the red curve in Figure 4.4, showed that the MCLs deflection increased when compared to the deflection produced by introducing equal concentrations of Hg^{2+} and Pb^{2+} (represented by the blue curve). The result of this experiment and the previous experiment (see section 4.2.2) also suggest that the presence of Pb^{2+} ions in the target solution prevent some of the Hg^{2} ions from binding

to the calix[4]arene host. This, in turn, would cause the generation of less surface stress on the MCL surface seen by the smaller deflection magnitude compared to the case where both target ions were injected subsequently (i.e. purple curves).

Results and Discussion of the Three Different Cases

The results of the first case —where the Pb^{2+} followed by Hg^{2+} — are incorporated into Figure 4.4 for comparison. Due to the length of time, the purple curve from Figure 4.3 was divided into two parts at the vertical dotted lines at the 10 and 40 minute points along the *x*-axis, indicating the introduction of each target ion to the fluid cell. This produces two approximately 30 minute periods of observation, represented by the two distinct and labelled purple curves, which start at the 10-minute mark on the *x*-axis in order to align with the observed timeframe (approximately 30 minutes each) of the other experiments.

When the experimental data are considered, two conclusions become apparent (Figure 4.4). First, the results indicate that the greater concentration of Hg^{2+} ions result in the greatest deflection. Second, the presence of other metal ions in the solution, in this case Pb^{2+} ions, affects the sensitivity of the triazole-calix[4]arene towards the Hg^{2+} ions as indicated by the magnitude of deflection.

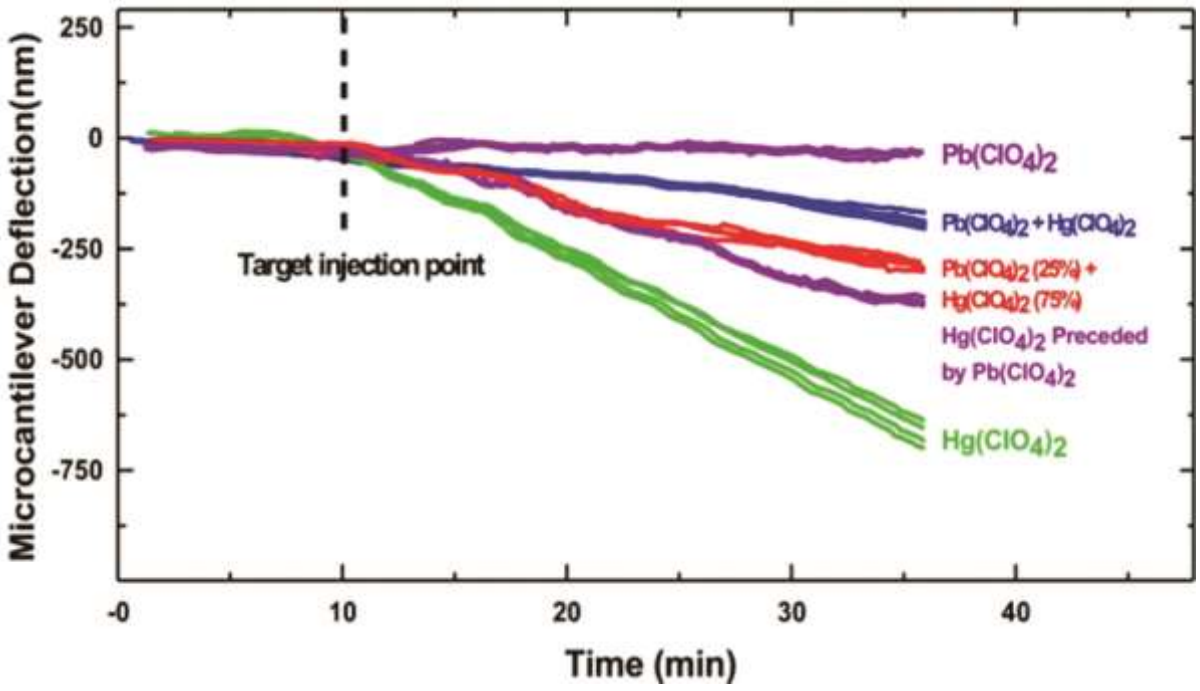

Figure 4.4: The results of different experiments that show the effect of the presence of Pb^{2+} ions on the sensitivity of the triazole-calix[4]arene functionalized MCLs towards Hg^{2+}.

These conclusions are supported by the sequential order of deflection resulting from different experiments (Table 4.2). The greatest deflection was a result for the 100% Hg^{2+} ion solution. The second largest deflection was for the case of Pb^{2+} followed by Hg^{2+} ion. The third largest deflection was for the solution containing a concentration of 75% Hg^{2+} ions and 25% Pb^{2+} ions. Next in largest deflection was for the result of a mixed solution of 50% Pb^{2+} and 50% Hg^{2+}. The experiment with the smallest deflection among these five was for the solution containing 100% Pb^{2+} ions (and thus 0% Hg^{2+} ions).

Table 4.2: The average MCL deflection at 35 min for triazole-calix[4]arene functionalized MCLs in the presence of Pb^{2+} and Hg^{2+} ions in solution.

Target	End Deflection (nm)
$Hg(ClO_4)_2$	-675.583
$Hg(ClO_4)_2$ Preceded by $Pb(ClO_4)_2$	-366.938
$Pb(ClO_4)_2$ (25 %) + $Hg(ClO_4)_2$ (75 %)	-309.042
$Pb(ClO_4)_2$ (50 %) + $Hg(ClO_4)_2$ (50 %)	-186.721
$Pb(ClO_4)_2$	-47.727

The experiment with 100% Hg^{2+} ions caused the greatest magnitude of deflection and the experiment with 0% Hg^{2+} ions (with 100% Pb^{2+} instead) caused the least deflection. When comparing curves of different experiments (Figure 4.4), the results revealed that the sensitivity of triazole-calix[4]arene functionalized MCLs towards Hg^{2+} ions varies. There was a decrease of approximately 44% as shown in Figure 4.4, in the MCL deflection in comparison with the case where Hg^{2+} ions were injected immediately after the fluid cell reached thermal equilibrium (green). When comparing to the case where a mixture of both 50 % Pb^{2+} and 50 % Hg^{2+} ions in a single solution (blue), the MCL deflection decreased by approximately 52% in comparison with the deflection produced by the sequential injection of 100% Pb^{2+} and 100% Hg^{2+} as shown above in Figure 4.4; whereas, it decreased by 87%

in comparison with the deflection that cause as a result of only 100% Hg^{2+} (green), as shown in Figure 4.4. While in the case of a mixture of 75% Hg^{2+} ions and 25% Pb^{2+} in a single solution (red), the MCL deflection increased in comparison to the solution with equal amounts of Hg^{2+} and Pb^{2+} (blue) (Figure 4.4).

The comparison of the results from the two experiments with the greatest deflection (i.e. comparing the purple and green data) (Figures 4.4) was useful for understanding the binding mechanism between the target ions and the triazole-calix[4]arene in the presence of different metal ions in the same solution. In the case where the Pb^{2+} followed by Hg^{2+}, the Pb^{2+} ions interacted with the triazole-calix[4]arene in such a way as to inhibit the interaction of the Hg^{2+} ions that were subsequently added. Our reasoning is that in the first injection of the Pb^{2+} solution, the Pb^{2+} would cover much or all of the MCL sensing layer, and in order for any great amount of Hg^{2+} to bind onto the sensing layer, it would have to displace some or all of the Pb^{2+}. We can therefore reason that since the results from Hg^{2+} preceded by Pb^{2+} were not the same as those from experiment for only 100% Hg^{2+}, there was still some Pb^{2+} bonded to the sensing layer and so not all of the Pb^{2+} ions may be displaced by the Hg^{2+} ions. We do know that some Pb^{2+} ions did bind to the MCL surface in the first injection of 100% Pb^{2+} experiment because a small deflection was produced.

4.3 The Sensitivity of Triazole-Calix[4]arene Functionalized MCLs to Different Types of Metal Ions

The response of triazole-functionalized MCLs to different metal ions was investigated in the next series of four experiments, which involved introducing 2×10^{-5} M aqueous

solutions of $Fe(ClO_4)_3$ ions, $Zn(ClO_4)_2$ ions, $Pb(ClO_4)_2$ ions, and $Ni(ClO_4)_2$ ions. All four experiments used the same experimental set up and procedures as outlined in the methodology section. In each experiment, arrays of triazole-calix[4]arene functionalized and reference MCLs were placed in the fluid cell and exposed to a continuous flow of DIW until an equilibrium state was reached. Next, each aqueous solution containing the target ion was injected into the MCLs and the MCL deflection was monitored for 35 minutes.

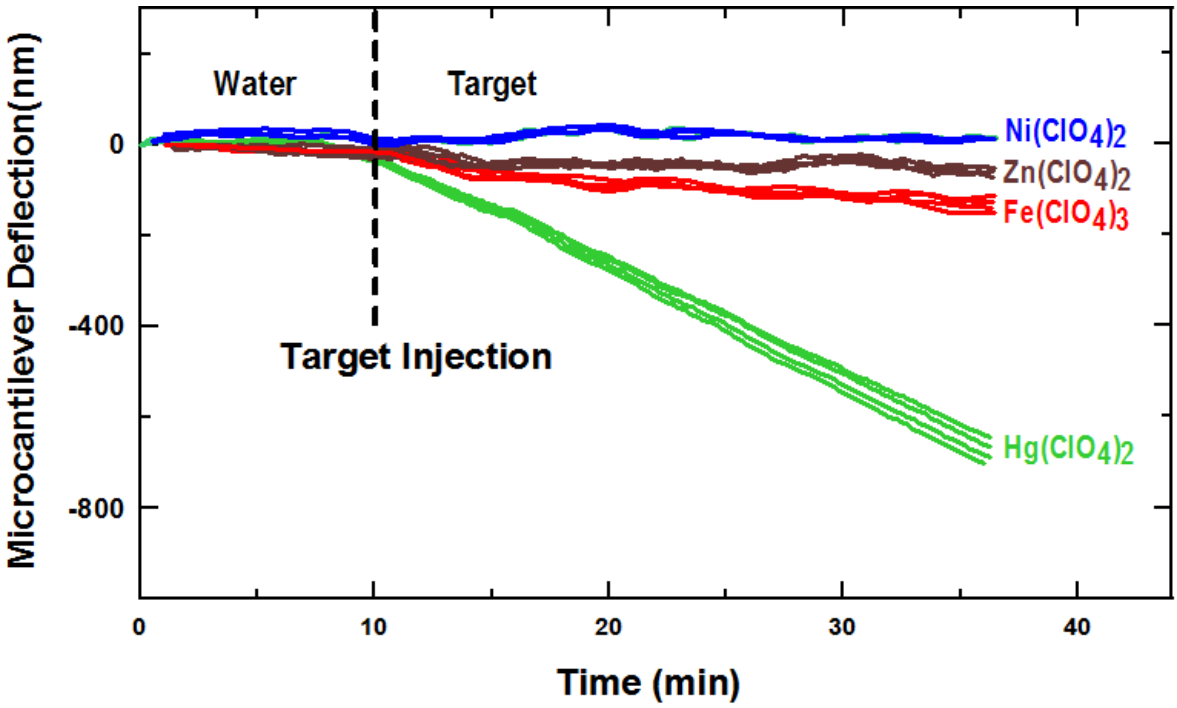

Figure 4.5: The MCLs response to the introduction of 2×10^{-5} M aqueous solutions of $Hg(ClO_4)_2$ (green), $Fe(ClO_4)_3$ (red), $Zn(ClO_4)_2$ (brown), and $Ni(ClO_4)_2$ (blue).

The results shown in Figure 4.5, indicate that the triazole-calix[4]arene functionalized MCLs have varyingly sensitive to different metal ions in aqueous solution, with the greatest sensitivity to mercury and the lowest sensitivity to nickel. The target solutions result in an

increasing deflection magnitude for different metal ions in the order of $Ni^{2+} < Pb^{2+} < Zn^{2+} < Fe^{3+}$, where the result of Pb^{2+} is represented in Figure 4.4.

The deflection magnitudes indicated that there was a low variation in the sensitivity for the functionalized MCLs between these four target metal ions. Each of the four experiments has the same concentration of 2×10^{-5} M of a single type of target metal ion, so the variation cannot be attributed to the concentration of metal ions or the influence of the presence of other metal ions in the target solution.

Our results for the different conducted experiments (i.e. different concentrations of mercury and mixed Pb^{2+} and Hg^{2+} solution) strongly support the conclusion that greater concentrations of Hg^{2+} ions result in the greatest deflection (Figure 4.4).

4.4 The Effect of Cations on the Sensitivity of Triazole-Calix[4]arene Functionalized MCLs

In order to better understand the molecular interactions between the target ions and the triazole-calix[4]arene functionalized MCL, it was necessary to investigate the effect of both the cation and anion. In a previous study conducted in our group, it was found that the sensitivity of calixarene-functionalized MCL sensors was attributed to both the cation and the anion [89].

Figure 4.5 illustrates that unlike the other target ions (i.e. Fe^{3+}, Ni^{2+}, Pb^{2+}, and Zn^{2+}), Hg^{2+} (denoted in green) shows the greatest deflection by a significant amount. This indicates that although the triazole-calix[4]arene functionalized MCL is responsive to other metal ions

(including Pb^{2+}, as presented in Figure 4.4), it is far more sensitive to Hg^{2+} than to any of the other target metal ion.

4.4.1 The Selectivity of Triazole-Calix[4]arene

As described above, the experimental results shown in Figure 4.5 indicated that triazole-calix[4]arene functionalized MCLs were more sensitive to some cations than others. The magnitude of the observed deflections for the different metal ions were found to be in following order: $Hg^{2+} > Fe^{3+} > Zn^{2+} > Pb^{2+} > Ni^{2+}$.

We were interested in determining which factors influence the magnitude of the MCL deflection. We first considered the possibility of the ionic radii of the target cations as the independent variable that produces the deflection results.

Despite the fact that factors such as the pH of the target solution and the entropy could affect the interaction between the calixarene and the target ions, there is general agreement in the literature that a major factor affecting the complexation between a calixarene receptor and metal ions is the ionic size [108]. We therefore examined whether the results we observed were a consequence of the size variation of the ionic radii of the target, or guest, ions (Ni^{2+}, Pb^{2+}, Zn^{2+}, Fe^{3+}, and Hg^{2+}) and the magnitude of the induced surface stress that results in the observed mechanical deflection of the functionalized MCLs.

The observed deflection was presumed to be due to the binding of the cations between the nitrogen atoms of the triazole functional groups of the host triazole-calix[4]arene which forms on the MCL. All of the cations except for Fe^{3+} are di-cations so apart from this one

which has three perchlorate counteranions, each of the others have only two perchlorate counteranions. Nevertheless, regardless of this consideration and comparing only the dications, there is no simple correlation between the deflection magnitudes with the ionic radii (Table 4.3). Therefore, the selectivity must be attributed to different influences including the electronic properties of the metals themselves (i.e. electron configuration and ionic size), which can impact the nature of the binding to the triazole moieties [109].

Table 4.3: The average deflection of triazole-calix[4]arene functionalized MCLs for 2.0×10^{-5} M concentrations of Hg^{2+}, Fe^{3+}, Zn^{2+}, Pb^{2+} and Ni^{2+} ions respectively.

Target	End Deflection (nm)	Ionic Radius (Å)
$Hg(ClO_4)_2$	-675.6	1.02
$Fe(ClO_4)_3$	-133.45	0.645
$Zn(ClO_4)_2$	-74.35	0.74
$Pb(ClO_4)_2$	-47.73	1.19
$Ni(ClO_4)_2$	-14.81	0.69

Reframing focus on the nature of the counteranions as an independent variable, would be a promising direction for future research. Further testing is required to determine the possible influence of the anions. We did not test this, which could be considered a limitation of our research; however, since the use of triazole-calix[4]arene-functionalized MCLs is a new area of study, there are many new areas open to examination and analysis to add to these initial experiments.

4.5 Discussion of Cantilever Saturation

The saturation state and the shape of the deflection curves are other interesting factors to consider; however, they go beyond the scope of the current research. In fact, the deflection curve and, in particular, the MCL saturation is a nontrivial issue and has been a subject of interest and investigation for us for a period of time. A previous publication by other members of our research group [89], discussed this issue and proposed several factors that have an effect on the deflection curve and the saturation state. Briefly, based on simple calculations and a review of the literature, they proposed that the notion of MCL saturation was related not only to the MCL itself but also to other factors [89]. For example, the geometry properties of the MCL sensor (i.e. thickness), the motion of target ions within the fluid cell and how they presented to the MCL are some of the factors that are significantly influence the saturation state [89].

4.6 Significance of Findings

Our research into the use of triazole-calix[4]arene functionalized MCLs provided several interesting findings. First, we determined that MCL arrays functionalized with triazole-calix[4]arene were capable of detecting trace concentrations of Hg^{2+} ions at extremely low concentrations. In our research, we detected Hg^{2+} ions as low as 10^{-11} M, which was sufficiently low for most applications, including testing water to determine if it meets or exceeds the limit of Hg^{2+} recommended by the Canadian environmental quality guidelines (see Table 2.1 for further detail).

Part II

Chapter 5 The New Functionalization Unit

5.1 Introduction

Part II of this dissertation presents original work focused on developing and testing a functionalization unit that was capable of *simultaneously* functionalizing eight individual MCLs within an array using microcapillary tubes.

5.2 Problem Context

Capillary-based functionalization is one of the best techniques that can be used for MCL functionalization for MCL arrays in comparison to other surface functionalization strategies [70]. Major advantages of using capillary-based functionalization are the ability to perform both parallel and individual functionalization of multiple MCLs, the ease of controlling the incubation time, and cost-effectiveness [110].

Moreover, capillary-based functionalization provides a uniform functionalization of the MCL surface with a high density of probe molecules, providing fast and reliable detection performance [70]. This was imperative because results are highly affected by the methodology used to immobilize probe molecules on the MCL surface [70]. Thus, it was

important to develop a unit that was capable of *simultaneously* functionalizing 8 individual MCLs within an array. While the functionalization unit previously developed required two steps to functionalize one 8-cantilever array, the new functionalization unit requires a single step, reducing the exposure time to ambient conditions and allowing experiments to be conducted quicker.

5.2.1 Technical Review

Previous Functionalization Unit Developed

Previous members of our group developed a functionalization unit that was capable of functionalizing only 4 MCLs with different sensing layers at one time (Figure 5.1).

With this unit, the functionalization procedure for one 8-MCL array was required to be conducted in two steps where four out of the eight MCLs in the array were functionalized at the same time as shown in Figure 5.1. In the end, this functionalization unit was able to produce 8 individually functionalized MCLs within a single array, with a process taking a total of 4 hours after the initial cleaning and preparation.

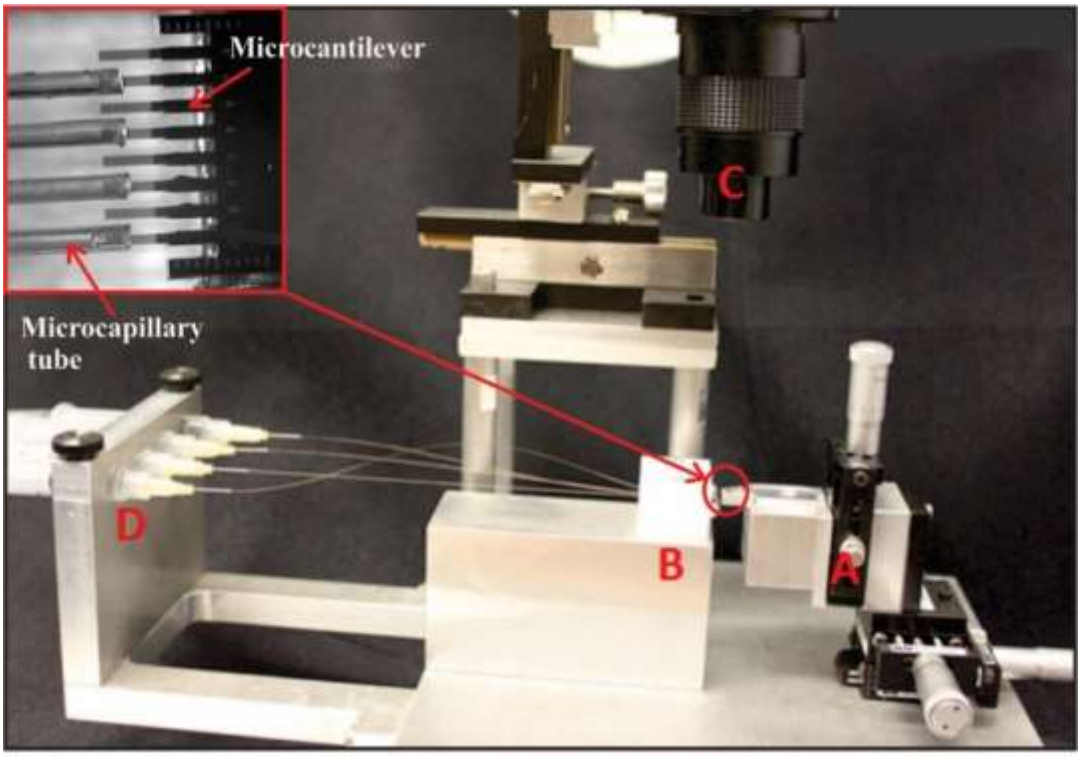

Figure 5.1: A photograph of the previous functionalization unit capable of functionalizing 4 MCL at one time. The main components of this system are: A) an XYZ translation stage, B) A support holder, C) An optical microscope, and D) 4 Syringes containing different solutions. The inset displays the insertion of four MCLs from the array into their corresponding capillary tubes. Reproduced with permission from [108].

There were several significant limitations to this method that may affect the formation of the sensing layers and the accuracy of subsequent experimental results. MCL surfaces are extremely sensitive to their surrounding environment and are contaminated in as little as 1 microsecond [58]. There were two significant periods of contamination during the procedure of using this functionalization unit. First, four of the eight MCLs were exposed

to the ambient conditions for 2h while the remaining four were incubated. Secondly, the freshly incubated MCLs were exposed to ambient conditions while the remaining MCLs were incubating for 2h. This thus created MCLs subjected to two different kinds of surface contaminations therefore creating fundamental differences in the sensors.

The second significant problem with our initial functionalization unit was with the syringes used to supply the incubation solution to the MCLs (Figure 5.2).

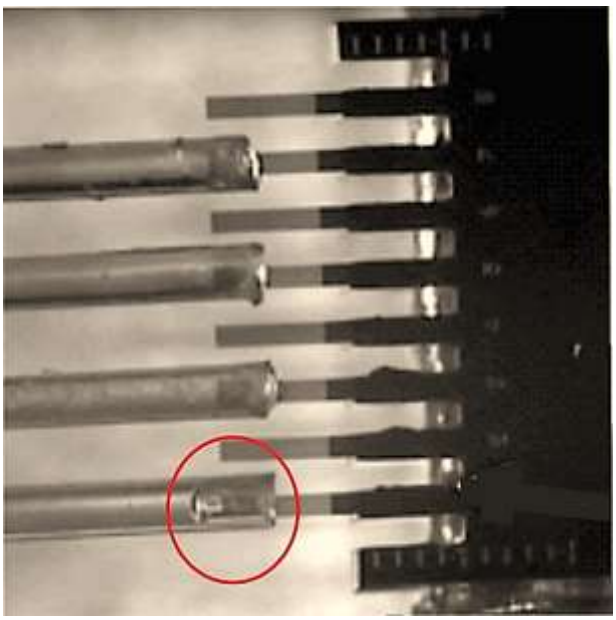

Figure 5.2: A photograph showing the relaxation of the target solution after the MCLs were inserted inside the microcapillary tubes during the incubation process. The red circle indicates where the solution was withdrawing into the microcapillary tube. Reproduced with permission from [108].

Through careful examination, it was found by me that there was a relaxation in the plunger after it was compressed into the syringe which cause the incubation solution to flow back into the microcapilary tubes (Figure 5.2), thereby limiting the exposure of the MCLs to the incubation solution. This effect, which had originally gone unnoticed, may very well have been the cause of irreproducible data observed by others in our group.

Therefore, because of the numerous limitations of our previous functionalization unit, a new one was designed by me and built by our machinist Gordon Whelan.

5.3 Design Description

In order to develop a better functionalization unit, the following requirements were established:

- Minimizing the risk of contaminating the MCLs;
- Maximizing the reproducibility when using the unit;
- Maintaining adequate saturation of the MCLs during the incubation period;
- Preventing the syringe plungers from relaxing;
- Prevent overflow causing cross contamination of the MCLs;
- A self-contained functionalization unit that does not require manual intervention during the incubation process;
- Functionalizing all 8 MCLs within the array at one time.

5.3.1 Detailed Description

The new 8 MCL functionalization unit was composed of several major components as illustrated in Figure 5.3.

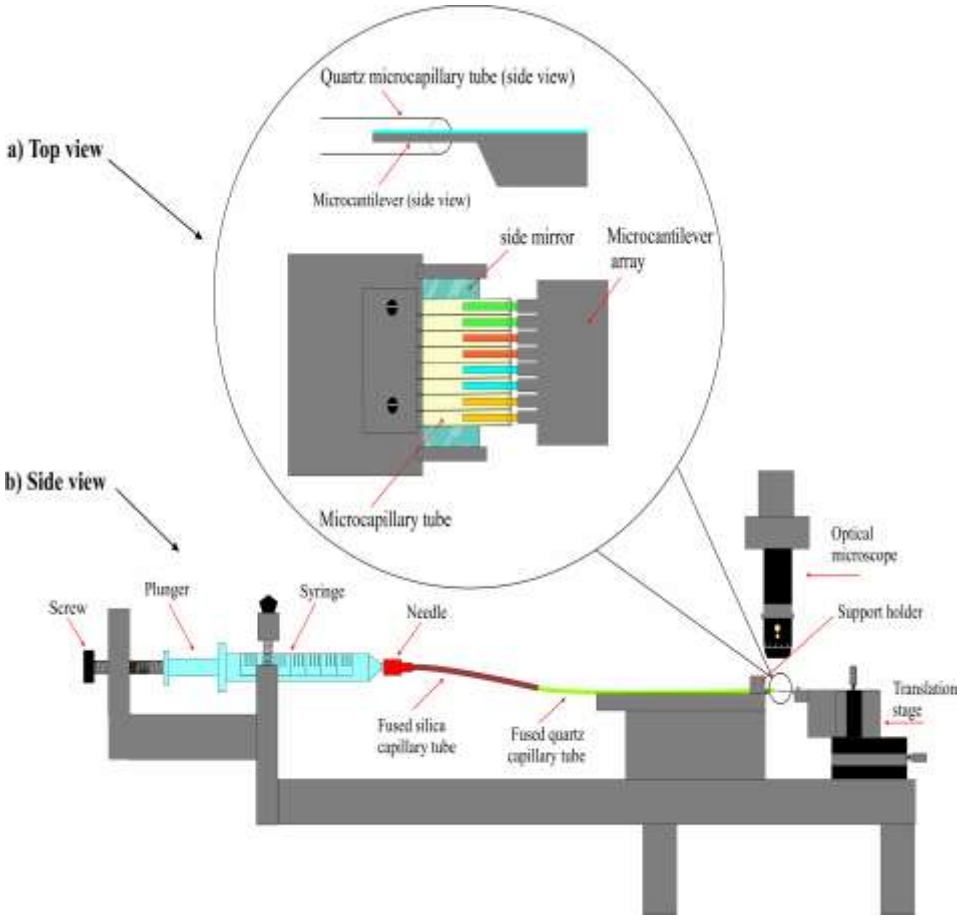

Figure 5.3: A schematic representation illustrating the side view of the new functionalization unit and its components. The plunger on each syringe was pushed and held in place by a thumb-screw. The target solution was introduced to the cantilevers through flexible silica tubes connected to narrower quartz microcapillary tubes. The MCL were inserted into the microcapillary tubes using an XYZ translation stage.

Eight syringes were used to supply different (same or any combination) functionalization solutions to the MCLs. The solutions were presented to the MCLs by turning a thumb screw which gently pushes the plunger. The screw then prevented the plunger from relaxing and maintained the solution at the very edge yet inside the tubes during the incubation process. Connected to the syringes were two different types of capillary tubes used to transport the functionalization solution to the MCL. A flexible silica tube with an outside diameter of 360µm ± 10µm and an inside diameter of 250µm ± 6µm was connected at one end to the needle of the syringe and at the other end to quartz tubes with an outside diameter of 240µm ± 25µm and an inside diameter of 180µm ± 25µm. These quartz tubes were held side-by-side as illustrated in Figure 5.3 and shown in Figure 5.4. The size of these quartz tubes, once placed side-by-side, were perfectly sized to allow all eight MCLs to fit inside the tubes. A support was used to hold the capillary tubes side-by-side. The support was held horizontally with a groove made to fit all eight quartz microcapillary tubes, side-by-side. An optical microscope was placed directly above the MCLs array, with right and left side view mirrors held at an angle of 45° under the MCLs array. The optical microscope and the mirrors were used to visualize the MCLs, to make sure that the MCLs were inserted properly inside the microcapillary tubes and to assure that the solution surrounded the MCLs. An XYZ translation stage, on which the MCL array was mounted, was used to align and insert the MCLs in the quartz capillaries.

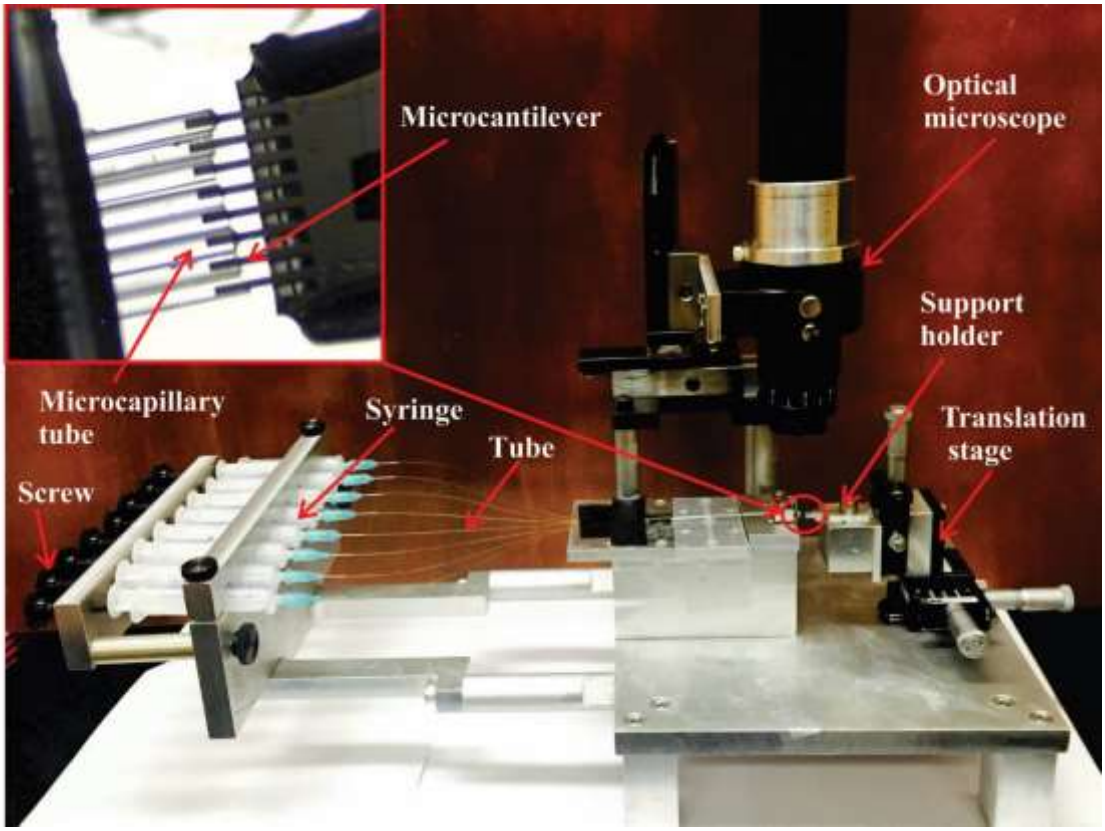

Figure 5.4: A photograph of the newly developed functionalization unit. The inset shows the suspended microcapillary tubes used to transport different functionalization solutions to the 8 MCL within an array, simultaneously.

System Verification

In order to assess that the functionalization unit was functioning properly, an experiment involving the simultaneous functionalization of different sensing layers was conducted. In this experiment, an array of 8 MCLs was prepared using the same cleaning and film deposition procedure as described in the methodology section of Part I. The gold-coated array was then transferred to the functionalization unit.

The 8 MCLs in the array were functionalized using 3 different types of sensing layers as indicated on Figure 5.5, with two MCLs of each type and two reference MCLs. The sensing layers selected were octanethiol, dodecanethiol, and triazole-calix[4]arene. The reason of such specific functionalization was to first investigate the effect of using different alkyl chain lengths (i.e.octanethiol) as the reference layer. In addition, two MCLs were left unfunctionalized because it was of interest to further investigate the potential binding between gold and Hg, which was observed in Figure 5.6, where the Au-coated MCL arrays showed larger deflections (green curves) than arrays functionalized with dodecanethiol and octanethiol (purple and blue curves respectively). The amalgamation between gold and mercury, which was observed by other researchers as well [107] indicates an area for further research.

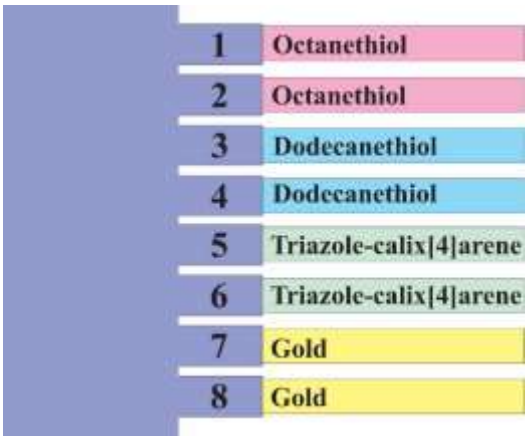

Figure 5.5: The functionalization scheme of the MCLs in the array for the initial test, MCLs 1 and 2 were coated with octanethiol, MCLs 3 and 4 were coated with dodecanethiol, MCLs 5 and 6 were functionalized with triazole-calix[4]arene while remaining MCLs 7 and 8 were left uncoated.

The MCLs were inserted into the microcapillary tubes and subjected to the functionalization solution for 2h. Monitoring the incubation period through the optical microscope indicated that the unit was able to maintain adequate saturation of the MCLs during the 2h period. No syringe relaxation or solution overflow was observed. Therefore, no manual intervention was required.

Following the functionalization process described previously, the MCL array was placed in the sensor cell and subjected to DIW until equilibrium was obtained. Following this a 2×10^{-5} M aqueous solution of Hg^{2+} was passed through the sensor cell at a flow rate of 0.1 ml/min for approximately 70 mins.

5.4 Results and Discussion

The MCL sensing results indicated that the greatest deflection was obtained from MCLs coated with triazole-calix[4]arene (results displayed in red), followed by gold (displayed in green), then dodecanethiol (purple), and octanethiol (blue) with the smallest observed deflection, as shown in Figure 5.6.

The triazole-calix[4]arene modified MCLs showed the greatest deflection over other MCLs in the array due to the higher sensitivity of the triazole-calix[4]arene towards Hg^{2+}. This high sensitivity was consistent with our previous results (Chapter 4, Part I). The deflection of the gold-coated MCLs is possibly due to the bonding between Au and Hg ions. The MCLs coated with different alkyl functional groups showed comparable deflections

suggesting that the MCL deflection was independent of chain length. This was consistent with others [79,111].

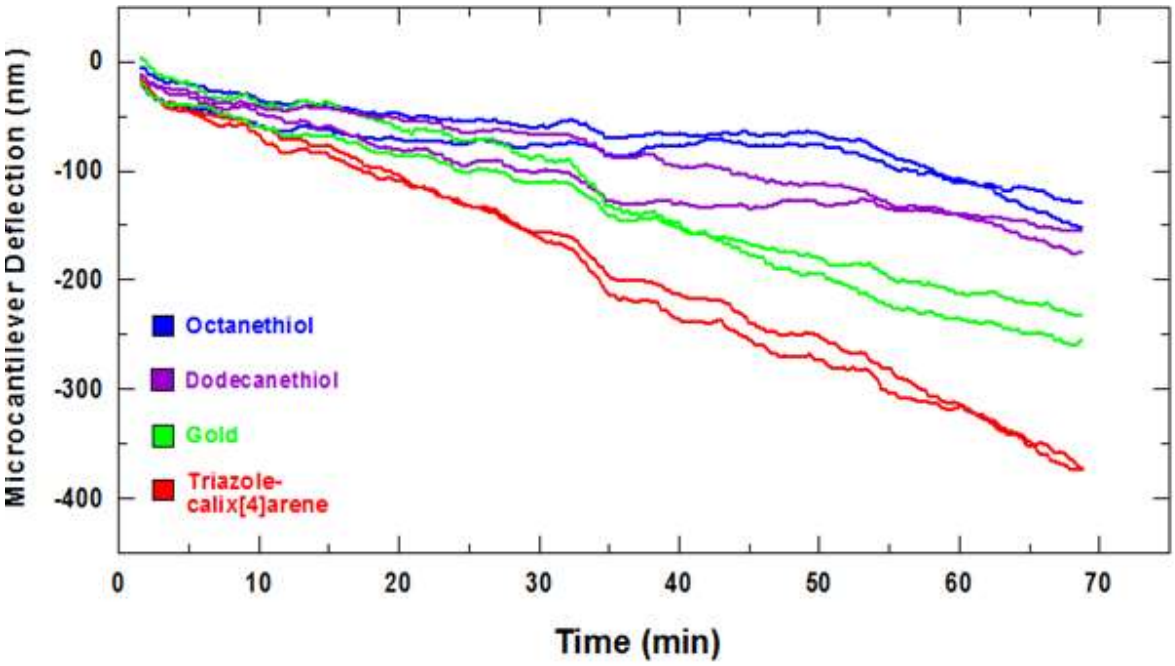

Figure 5.6: Cantilever deflection versus time curves for testing the new functionization triazole-calix[4]arene (red), left uncoated (green), dodecanethiol (purple), and octanethiol (blue) and then exposed to 2×10^{-5} M aqueous solution of Hg^{2+}.

The slight spreading of the deflection curves is due to the slight difference in the spring constant of the different MCLs across the arrays as shown in [93]. Unfortunately, we had not measured the spring constants of the MCLs in order to normalize the MCL sensor data by plotting them in units of surface stress instead of MCL deflections. In the same way, it is not possible to compare these results to those shown in chapter 4 because neither data was expressed in terms of surface stress. Although sensing experiments shown in Figure

4.1 gave significantly larger MCL deflections, they may have been conducted with MCLs with smaller spring constants.

The use of this new functionalization unit requires dexterity and skill and must be performed carefully. The delicate process of adjusting the array's position with the XYZ translation stage and sliding the MCLs inside the microcapillary tubes takes approximately 20 minutes. During this time, the surface of the cleaned and gold coated MCLs were exposed to contaminants in the air. This was significant because of the important role of probe molecule density on the MCLs surface layer. Contaminants act as barriers when they cover the MCL surface so that the gold surface accessible to the probe molecules was reduced. This, in turn, may limit the degree of self-assembly on the surface of Au-coated MCLs, and reduces the capture efficiency of molecular absorption, ultimately leading to reduced surface stress generation. Haag *et al*. notes that interfering with the interaction between the probe molecules and the gold surface impacts not only the accuracy of results, but also the response time [58]. Perhaps in the future it may be necessary to investigate keeping the gold-coated MCL under a flow or argon gas as they are positioned into the capillary tubes.

Chapter 6 Conclusions

6.1 Dissertation Conclusions

In Part I of this dissertation, results showed that triazole-calix[4]arene functionalized MCL sensors were capable of detecting heavy metals in aqueous solutions. The presence of metal ions was determined by monitoring the mechanical deflection of the functionalized MCLs. Experiments were carried out in an experimental set up that allows two arrays each consisting of eight functionalized MCLs to be simultaneously monitored. The mechanical deflection of the MCLs was measured using an optical beam deflection system (OBDS). The sensitivity of triazole-calix[4]arene towards different concentrations of mercury was tested determining that higher concentrations of Hg^{2+} results in proportionally higher deflection magnitude.

Additional experiments were also conducted to investigate the effect of the presence of Pb^{2+} ions on the sensitivity of the triazole-calix[4]arene towards Hg^{2+}. The results indicated that the sensitivity of triazole-calix[4]arene towards Hg^{2+} was decreased when Pb^{2+} ions was presented in the same solution. This indicated that the triazole-calix[4]arene functionalized MCLs were able to interact with two distinct types of metal ions in the same solution, with varying sensitivity.

Moreover, experiments were conducted to investigate the sensitivity of triazole-clix[4]arene towards different metal ions and results showed that the triazole-calix[4]arene was able to detect other metal ions, such as Fe^{3+}, Ni^{2+}, Zn^{2+}, and Pb^{2+}, in aqueous solutions. Ultimately, the experimental data supported the conclusion that triazole-calix[4]arene has a higher sensitivity towards Hg^{2+} ions than the other metal ions tested.

In Part II of this dissertation, the new functionalization unit was built which allows 8 MCLs in an array to be modified with 8 different sensing layers at the same time, ensuring identical experimental conditions and increasing the reliability of our results. The new system included screws to fix the plungers in position. This prevents syringe relaxation preventing the functionalizing solution from withdrawing from the MCLs during the incubation. This modification also ensures that the MCLs were fully saturated throughout the 2h incubation period, improving the consistency and accuracy of results.

Experimental testing of the new functionalization unit showed that smaller MCL deflections were observed then those obtained when the array was submerged directly into the triazole-calix[4]arene solution. However, because the data were not shown in terms of surface stress it is impossible to accurately compare the data. The research conducted for Part I and Part II of this dissertation contributes to a foundation for the future development of reliable, portable, and easy-to-use devices for the highly sensitive detection and quantification of mercury in aqueous solutions and for the detection of multiple heavy metals in aqueous solutions.

6.2 Directions for Future Research

There are multiple directions for future research for improving triazole-calix[4]arene sensing layers to more accurately detect and distinguish multiple types of metal ions in the same solution. One possible solution to improve the selectivity of calix[4]arene compounds is to modify them with highly selective functional groups such as chelators that would bind more selectively to particular metal ions, such as Hg^{2+}, Fe^{3+}, and Cu^{2+}ions [112].

One of the potential and important future work is to investigate the effect of the exposed Au between the calixarene molecules. When the calixarene molecules assemble onto the gold surface, some of gold surface will be exposed. As the target ion is introduced, some of these ions interact with the calixarene molecules and other will interact with the exposed gold surface. As an example of these interactions, a recent study confirmed that iodide ions (I^-) can chemisorb onto the gold surface and since these interactions are strong, surface stress on the gold surface can be induced [113]. Therefore, it is crucial in future studies to account for these interactions and find a method of calculating the deflection produced by ions interaction with the exposed gold surface. One possibility is to attempt to eliminate these potential interactions by depositing thiols between the calixarene molecules. In our study, we have found that the deflection magnitude produced by the interactions between target ions and thiol deposited on the gold surface (i.e. reference microcantilever) is very small. Thus, the co-deposition of thiols with calixarene molecules can, in principle, be used to reduce the effect of target ions reacting with the exposed gold atoms.

While some contamination was inevitable, controlling and minimizing exposure to sources of contamination was a high priority. Therefore, another direction for future research into the improvement of a simultaenous funcitonalization unit is to explore the possibility of controlling contamination from the ambient air by conducting the functionalization process within a clean enviroment such as a stream of Ar gas.

Additional important work to be conducted is to investigate the exposure time of MCLs surface to ambient air condition for different periods of time. By doing this we can hopefully gain a deeper understanding of how the exposure time affects the quality of calixarene SAM on the gold surface and the corresponding deflection magnitude, and lastly the reliability of the experimental results.

Furthermore, the incubation time of the MCLs in the triazole-calix[4]arene solution has a direct effect on the sensitivity and thus the deflection magnitude as have shown by others [108]. Therefore, investigating the variation of incubation time using the new functionalization unit should be considered for future work in order to optimize the sensor sensitivity.

References

1 Alodhayb AN, Braim M, Beaulieu LY, Valluru G, Rahman S, Oraby AK, Georghiou PE. Metal Ion Binding Properties of a Bimodal Triazolyl-Functionalized Calix[4]arene on a Multi-Array Microcantilever System. Synthesis, Fluorescence and DFT Computation Studies. RSC Advances. 2016;6(6):4387-4396.

2 Ongley, E. D.; Food and Agriculture Organization of the United Nations. Control of water pollution from agriculture. Rome: Food and Agriculture Organization of the United Nations; 1996.

3 The Hospital for Sick Children; University of Toronto. Analytical Methods for Heavy Metals in the Environment: Quantitative Determination, Speciation, and Microscopic Analysis. In: Sarakar B, editor. Heavy Metals in the Environment. New York: Dekker; 2002. p. 35-40.

4 Ewing KJ(RL), Nau GM, Jaganathan J, Bilodeau TG, Schneider I, Aggarwal ID. Detection of trace levels of mercury in aqueous systems via a fiber optic probe. In: Chemical, Biochemical, and Environmental Fiber Sensors V; 1994. p. 286-295.

5 Mayr T. Optical Sensors for the Determination of Heavy Metal Ions. Doctoral Thesis. Regensburg: University of Regensburg; 2002.

6 Duffus JH. "Heavy Metals"--A Meaningless Term? Pure Appl. Chem. 2002;74(5):793-807.

7 Ilic B, Yang Y, Craighead HG. Virus detection using nanoelectromechanical devices. 2004;85(2604).

8 Duruibe JO, Ogwuegbu MOC, Egwurugwu JN. Heavy metal pollution and human biotoxic effects. Int. J. Phys. Sci. 2007;2(5):112-118.

9 Singh R, Neetu G, Mishra A, Gupta R. Heavy metals and living systems: An overview. Indian Journal of Pharmacology. 2011;43(3):246-253.

10 Nazir R, Khan M, Masab M, Rehman HU, Rauf NU. Accumulation of Heavy Metals (Ni, Cu, Cd, Cr, Pb, Zn, Fe) in the soil, water and plants and analysis of physico-chemical parameters of soil and water Collected from Tanda Dam kohat. Journal of Pharmaceutical Sciences and Research. 2015;7(3):89-97.

11 Adefris Adal MM, Sage W. Wiener M. Heavy Meal Toxicity: Background. [Internet]. 2016 [cited 2016 July 22]. Available from: http://emedicine.medscape.com/article/814960-overview.

12 Järup L. Hazards of heavy metal contamination. British Medical Bulletin. 2003;68:167-182.

13 National Institutes of Health: Office of Dietary Supplements. Lead Fact Sheet for Health Professionals. [Internet]. 2016 [cited 2016 July 24]. Available from: https://ods.od.nih.gov/factsheets/Iron-HealthProfessional/.

14 National Institutes of Health: Office of Dietary Supplements. Zinc Factsheet for Health Professionals. [Internet]. 2016 [cited 2016 July 22]. Available from: https://ods.od.nih.gov/factsheets/Zinc-HealthProfessional/#h2.

15 U.S. Department of the Interior-U.S. Geological Survey. Mercury Contamination of Aquatic Ecosystems [Fact Sheet]. Fact Sheet FS-216-95. US Geological Survey; 2016.

16 Harada M. Minamata Disease: Methylmercury Poisoning in Japan Caused by Environmental Pollution. Critical Reviews in Toxicology. 1995;25(1):1-24.

17 Sauve L. The Ghosted City: Unrepresented X-Factors. In: The Mediated City Conference; 2014; London.

18 Broughton E. The Bhopal disaster and its aftermath: a review. Environ. Health. 2005;4(6):6-6.

19 Giger W. The Rhine red, the fish dead—the 1986 Schweizerhalle disaster, a retrospect and long-term impact assessment. Environ Science and Technology in Romania. 2009.

20 Guerrero FM, Lozano M, Rueda-Cantuche JM. Spain's greatest and most recent mine. Overseas Development Institute Journal Compilation. 2007.

21 Krafta C, jr. WvT, Zachmanna DW. The effects of mining in Northern Romania on the heavy metal distribution in sediments of the rivers Szamos and Tisza (Hungary). Acta Hydrochim. Hydrobiol. 2006;34:257-264.

22 Törmä H, Kujala S, Kinnunen J. The employment and population impacts of the boom and bust of Talvivaara mine in the context of severe environmental accidents – A CGE evaluation. Resources Policy. 2015;46:127-138.

23 Petticrew EL, Albers SJ, Baldwin SA, Carmack EC, Déry SJ, Gantner N, Graves KE, Laval B, Morrison J, Owens PN, et al. Aquatic impacts of an environmental disaster in a relatively pristine watershed: the breach of the Mount Polley Mine tailings impoundment, British Columbia, Canada. Geophysical Research Letters. 2015;42:3347-3355.

24 Fiscor S. Gold King Spill Daylights EPA's Poor Remediation Practices. Engineering and Mining Journal. 2015;216(9):66-68.

25 Canadian Council of Ministers of the Environment. Canadian Water Quality Guidelines for the Protection of Aquatic Life: Inorganic Mercury and Methylmercury. In: Canadian Environmental Quality Guidelines. Winnipeg: Environment Canada; 2003.

26 Environment and Climate Change Canada. Canadian Environmental Sustainability Indicators: Releases of Harmful Substances to the Environment. Environment and Climate Change Canada; 2016. Available from: http://www.ec.gc.ca/indicateurs-indicators/default.asp?lang=en&n=3C4C1124-1.

27 Mousavi A, Chávez RD, Ali AMS, Cabaniss SE. Mercury in Natural Waters: A Mini-Review. Environmental Forensics. 2011;12(1):14-18.

28 Gochfeld M. Cases of Mercury Exposure, Bioavailability, and Absorption. Ecotoxicology and Environmental Safety. 2003;56(1):174-179.

29 Michigan Mercury Pollution Prevention Task Force. Mercury Pollution Prevention in Michigan: Summary of Current Efforts and Recommendations for Future Activities. Michigan Department of Environmental Quality; 1996.

30 Kathryn R. Mahaffey; U.S. Environmental Protection Agency. Fish and shellfish as dietary sources of methylmercury and the o-3 fatty acids, eicosahexaenoic acid and docosahexaenoic acid: risks and benefits. Environmental Research. 2004;95:414-428.

31 Risher JF, Amler SN. Mercury Exposure: Evaluation and Intervention The Inappropriate Use of Chelating Agents in the Diagnosis and Treatment of Putative Mercury Poisoning. Neurotoxicology. 2005;26:691-699.

32 Harrison RM, Laxen DPH. Control of Lead Discharges to Water. In: Lead Pollution: Causes and Control. 1st ed. Springer Netherlands; 1981. p. 104-132.

33 Hong-bo L, Chne K, Juhasz AL, Huang L, Ma LQ. Childhood Lead Exposure in an Industrial Town in China: Coupling Stable Isotope Ratios with Bioaccessible Lead. Environmental Science and Technology. 2015;49:5080-5087.

34 Agency for Toxic Substances and Disease Registry. Toxicological Profile for Lead: Health Effects. Toxicological Profile. Public Health Service; 2007.

35 Cempel M, Nikel G. Nickel: A Review of Its Sources and Environmental Toxicology. Polish Journal of Environmental Studiess. 2006;15(3):375-382.

36 Keim W. Nickel: An Element with Wide Application in Industrial Homogenous Catalsis. Angew. Chem. Int. Ed. Engl. 1990;29:235-244.

37 R. Eisler; Patuxent Wildlife Research Center. Nickel Hazards to Fish, Wildlife, and Invertebrates: A synoptic Review. Contaminant Hazard Reviews Report. National Technical Information Service; 1998.

38 Grimsrud TK, Berge SR, Haldorsen T, Anderson A. Exposure to Different Forms of Nickel and Risk of Lung Cancer. American Journal of Epidemiology. 2002;156(12):1123-1132.

39 Task Force on Water Quality Guidelines. Water Quality Guidelines for the Protection of Aquatic Life: Freshwater, Marine. Winnipeg: Manitoba Statutory Publications; 1999 Canadian Council of Ministers of the Environment.

40 García R, Báez AP. Atomic Absorption Spectroscopy (AAS). In: Farrukh MA, editor. Atomic Absorption Spectroscopy. InTech; 2011. p. 1-12.

41 Fei H, Barron AR. Ion Selective Electrode. [Internet]. 2012 [cited 2016 Jul 22]. Available from: http://cnx.org/contents/fd875986-2c51-4366-8e96-ad4cf7310184@1.

42 Kahlert H. Potentiometry. In: Scholz F, editor. Electroanalytical Methods: Guide to Experiments and Applications. 2nd ed. Springer; 2002. p. 237-256.

43 Henn D, Cammann K. Voltammetric Ion-Selective Electrodes (VISE). Electroanalysis. 2000;12(16):1263-1271.

44 Lindner E, Pendley BD. A Tutorial on the Application of Ion Selective Electrode Potentiometry. Analytica Chimica Acta. 2013;762:1-13.

45 Boisen A, Dohn S, Keller SS, Schmid S, Tenje M. Cantilever-like Micromechanical Sensors. Reports on Progress in Physics. 2011;74(3).

46 Llic B, Yang Y, Craighead H. Virus Detection Using Nanoelectromechanical Devices. Applied Physics Letters. 2004;85(13):2604-2606.

47 Using Microcantilever Deflection to Detect HIV-1 Envelope Glycoprotein gp120. Nanomedicine. 2006;2(4):222-229.

48 Etayash H, Jiang K, Azmi S, Thundat T, Kaur K. Real-time Detection of Breast Cancer Cells Using Peptide-functionalized Microcantilever Arrays. Nature. 2015;5(13967).

49 Raiteri R, Grattarola M, Butt HJ, Skládal P. Micromechanical Cantilever-based Biosensors. Sensors & Actuators: B. 2001;79(2):115-126.

50 Berger R, Delamarche E, Lang HP, Gerber C, Gimzewski JK, Meyer E, Güntherodt HJ. Surface Stress in the Self-Assembly of Alkanethiols on Gold. Science. 1997;276(5321):2021-2024.

51 Yang YT, Callegari C, Feng XL, Ekinci KL, Roukes ML. Zeptogram-Scale Nanomechanical Mass Sensing. Nano Letters. 2006;6(4):583.

52 Alvarez M, Carrascosa LG, Moreno M, Calle A, Zaballos A, Lechuga LM, Martinez C, Tamayo J. Nanomechanics of the Formation of DNA Self-Assembled Monolayers and Hybridization on Microcantilevers. Langmuir. 2004;20:9663-9668.

53 Senesac L, Thundat TG. Nanosensors for Trace Explosive Detection. Materials Today. 2008;11(3):28-36.

54 Cherian S, Gupta RK, Mullin BC, Thundat T. Protein-Functionalized, Detection of Heavy Metal Ions Using Protein-Functionalized Microcantilever Sensors. Biosensors and Bioelectronics. 2003;19(5):411-416.

55 Brattoli M, De Gennaro G, De Pinto V, Loiotile AD, Lovascio S, Penza M. Odour Detection Methods: Olfactometry and Chemical sensors. Sensors. 2011;11(5):5290-2322.

56 Lavrik NV, Sepaniak MJ, Datskos PG. Cantilever Transducers as a Platform for Chemical and Biological Sensors. Review of Scientific Instruments. 2004;75(7):2229-2253.

57 Vashist SK. A Review of Microcantilevers for Sensing Applications. AZoNano. 2007;3:1-18.

58 Haag AL, Nagai Y, Lennox R, Grütter P. Characterization of a Gold Coated Cantilever Surface for Biosensing Applications. EPJ Techniques and Instrumentation. 2015;2(1):1-12.

59 Athamneh AiM, Cartagena-Rivera Ax, Raman A, Suter Dm. Substrate Deformation Predicts Neuronal Growth Cone Advance. Biophysical Journal. 2015;109(7):1358-1371.

60 Haag AL. Potential-Driven Surface Stress of a Cantilever-Based Sensor. Doctoral Dissertation. Montreal, Canada: McGill University; 2016.

61 Zhang HY, Pan HQ, Zhang BL, Tang JL. Microcantilever Sensors for Chemical and Biological Applications in Liquid. Chinese Journal of Analytical Chemistry. 2012;40(5):801-808.

62 Tamayo J, Humphris ADL, Malloy AM, Miles MJ. Chemical sensors and biosensors in liquid environment based on microcantilevers with amplified quality factor. Ultramicroscopy. 2001;86(1):167-173.

63 Beaulieu LY, Godin M, Laroche O, Tabard-Cossa V, Grütter P. A Complete Analysis of the Laser Beam Deflection Systems Used in Cantilever-Based Systems. Ultramicroscopy. 2007;107(4):422-430.

64 Lang H, Gerber C. STM and AFM Studies on (Bio)molecular System: Title: STM and AFM Studies on (Bio)molecular Systems: Unravelling the Nanoworld. Berlin, Heidelberg: Springer Berlin Heidelberg; 2008. p. 1-27.

65 Goeders KM, Colton JS, Bottomley LA. Microcantilevers: Sensing Chemical Interactions via Mechanical Motion. Chemical Reviews. 2008;108(2):522-542.

66 Waggoner PS, Craighead HG. Micro- and Nanomechanical Sensors for Environmental, Chemical, and Biological Detection. 2007;7(10):1238-1255.

67 Osiander R DMCJ, editor. MEMS and Microstructures in Aerospace Applications. CRC press; 2005.

68 Kovacs GTA, Maluf NI, Petersen KE. Bulk Micromachining of Silicon. Proceedings of the IEEE. 1998;86(8):1536-1551.

69 Lang H, Hegner M, Gerber C. Cantilever Array Sensors. Materials Today. 2005;8(4):30-36.

70 Chaudhary M, Gupta A. Microcantilever-based Sensors. Defence Science Journal. 2009;59(6):634-641.

71 Korotcenkov G, Vashist S. Chemical Sensors: Comprehensive Sensor Technologies. New York: Momentum Press; 2011. p. 321-332.

72 Tundat T. Trace Chemical Sensing of Explosives. 1st ed. Vol 31. New Jersey: John Wiley & Sons; 2007.

73 Dhayal B. Silicon Microcantilevers as Sensors. Doctoral dissertation. West Lafayette, Indiana: Purdue University; 2007. 3307400.

74 Shiba K, Imamura G, Yoshikawa G. Biomaterials Nanoarchitectonics. 1st ed. Elsevier; 2016.

75 Godin M. Surface Stress, Kinetics, and Structure of Alkanethiol Self-Assembled Monolayers. Doctoral dissertation. Montréal, Canada: McGill University; 2004.

76 Wu G, Ji H, Hansen K, Thundat T, Datar R, Cote R, Hagan MF, Chakraborty AK, Majumdar A. Origin of Nanomechanical Cantilever Motion Generated from Biomolecular Interactions. Proceedings of the National Academy of Sciences of the United States of America. 2001;98(4):1560-1564.

77 Godin M, Williams PJ, Tabard-Cossa V, Laroche O, Beaulieu LY, Lennox RB, Grütter P. Surface Stress, Kinetics, and Structure of Alkanethiol Self-Assembled Monolayers. Langmuir. 2004;20(17):7090–7096.

78 Xie R. Theoretical Study on Adsorbate-Induced Surface Stress in the Self-Assembly of Alkanethiols on Gold. Surface Review and Letters. 2009;16(6):807-814.

79 Godin M, Tabard-Cossa V, Miyahara Y, Monga T, Williams PJ, Beaulieu LY, Bruce Lennox R, Grutter P. Cantilever-Based Sensing: the Origin of Surface Stress and Optimization Strategies. Nanotechnology. 2010;21(7).

80 Fred A, Filipe J, Gamboa H, editors. Biomedical Engineering Systems and Technologies. Vol 127. Dordrecht : Springer; 2011.

81 Herrero E, Buller LJ, Abruña HD. Underpotential Deposition at Single Crystal Surfaces of Au, Pt, Ag and other Materials. Chemical Reviews. 2001;101(7):1897-1930.

82 Georghiou PE, Li ZH, Ashram MO, Chowdhury SO, Mizyed SO, Tran AO, Al Saraierh HO, Miller DO. Calixnaphthalenes: Deep, Electron-Rich Naphthalene Ring-Containing Calixarenes. The First Decade. Synlett. 2005 0879-0891.

83 Gutsche CD. Calixarenes : An introduction. 2nd ed. The Royal Society of Chemistry; 2008.

84 Gokel GW, Koga K. United States-Japan Seminar on Host-Guest Chemistry. Vol 7. Dordrecht ; Boston: Kluwer Academic Publishers; 1989.

85 Asfari Z, Bohmer V, Harrowfield J, Vicens J, editors. Calixarenes 2001. 1st ed. Boston: Springer Science & Business Media; 2007.

86 Mandolini L, Ungaro R, editors. Calixarenes in Action. World Scientific; 2000.

87 Abd-el-aziz AS, Shipman PO, Pilfold JL, Shipley PR. Synthesis of Upper Rim Functionalized Calixarene-Based Poly(norbornenes. Macromolecular Chemistry and Physics. 2010;211(9):996-1002.

88 Arora V, Chawla HM, Singh SP. Calixarenes as Sensor Materials for Recognition and Separation of Metal Ions. Arkivoc. 2007;2007(2):172-200.

89 Alodhayb A, Saydur Rahman SM, Rahman S, Valluru GK, Georghiou PE, Beaulieu LY. Detection of Calcium Ions Using Gold-Coated Micro-Cantilever Sensors Using Upper- and Lower-Rim Functionalized Calix[4]arenes. Sensors & Actuators: B. Chemical. 2014;203:766-773.

90 Georghiou PE, Rahman S, Valluru G, Dawe LN, Rahman SMS, Alodhayb AN, Beaulieu LY. Synthesis of an Upper - and Lower -Rim Functionalized Calix[4]arene for Detecting Calcium Ions Using a Microcantilever Sensor. New Journal of Chemistry. 2013;37(5):1298-1301.

91 Kim HJ, Lee MH, Mutihac L, Vicens J, Kim JS. Host-Guest Sensing by Calixarenes on the Surfaces. Chemical Society reviews. 2012;41(3):1173-1190.

92 Samanta K, Rao CP. A Bifunctional Thioether Linked Coumarin Appended Calix4arene Acquires Selectivity Toward Cu(2+) Sensing on Going from Solution to SAM on Gold. ACS applied materials & interfaces. 2016;8(5):3135-3142.

93 Alodhayb A, Rahman SMS, Rahman S, Georghiou PE, Beaulieu LY. A 16-Microcantilever Array Sensing System for the Rapid and Simultaneous Detection of Analyte. Sensors & Actuators: B. 2016;237:459-469.

94 Valluru G, Rahman S, Georghiou PE, Dawe LN, Alodhayb AN, Beaulieu LY. Synthesis of a Cone -Conformer Bimodal Calix[4]arene-Crown-5 which Forms a Sensitive Cesium Ion Sensing Layer on Gold-Coated Microcantilevers. New Journal of Chemistry. 2014;38(12):5868-5872.

95 Sheller NB, Petrash S, Foster MD, Tsukruk VV. Atomic Force Microscopy and X-ray Reflectivity Studies of Albumin Adsorbed onto Self-Assembled Monolayers of Hexadecyltrichlorosilane. Langmuir. 1998;14(16):4535–4544.

96 Samant MG, Brown CA, Gordon JG. Structure of an Ordered Self-Assembled Monolayer of Docosyl Mercaptan on Gold(111) by Surface X-ray Diffraction. Langmuir. 1991;7(3):437–439.

97 Ulman A. Formation and Structure of Self-Assembled Monolayers. Chemical reviews. 1996;96(4):1533-1554.

98 Janssen D, De Palma R, Verlaak S, Heremans P, & Dehaen W. Static Solvent Contact Angle Measurements, Surface Free Energy and Wettability Determination of Various Self-Assembled Monolayers on Silicon Dioxide. Science Direct. 2006;515(4):1433–1438.

99 Chaki NK, Vijayamohanan K. Self-Assembled Monolayers as a Tunable Platform for Biosensor Applications. Biosensors and Bioelectronics. 2002;17(1):1–12.

100 Pandya HJ, Kim HT, Roy R, Desai JP. MEMS Based Low Cost Piezoresistive Microcantilever Force Sensor and Sensor Module. Materials Science in Semiconductor Processing. 2014;19:163-173.

101 Taylor RF, Schultz JS, editors. Handbook of Chemical and Biological Sensors. 1st ed. CRC Press; 1996.

102 Love JC, Estroff LA, Kriebel JK, Nuzzo RG, Whitesides GM. Self-Assembled Monolayers of Thiolates on Metals as a Form of Nanotechnology. Chemical reviews. 2005;105(4):1103-1170.

103 Alodhayb A, Brown N, Saydur Rahman SM, Harrigan R, Beaulieu LY. Towards Detecting the Human Immunodeficiency Virus Using Microcantilever Sensors. Applied Physics Letters. 2013;102(7).

104 Mishra R, Grange W, Hegner M. Rapid and Reliable Calibration of Laser Beam Deflection System for Microcantilever-Based Sensor Setups. Journal of Sensors. 2012;2012:1-6.

105 Manning KY, Butt NR, Alodhayb A, Saika-Voivod I, Beaulieu LY. Modeling the motion and detection of particles in microcantilever sensor cells. Journal of Applied Physics. 2013;113(11).

106 Li SS, Xu LP, Wan LJ, Wang ST, Jiang L. Time-Dependent Organization and Wettability of Decanethiol Self-Assembled Monolayer on Au(111) Investigated with STM. The journal of physical chemistry. B. 2006;110(4):1794-1799.

107 Xu X, Thundat TG, Brown GM, Ji HF. Detection of Hg2+ Using Microcantilever Sensors. Analytical chemistry. 2002;74(15):3611-3615.

108 Alodhayb A. Development of Calix[4]arene-Functionalized Microcantilever Array Sensing System for the Rapid, Sensitive and Simultaneous Detection of Metal Ions in Aqueous Solutions. Doctoral dissertation. St. John's, Canada: Memorial University of Newfoundland; 2016.

109 Perez Holmberg J. Competitive Adsorption and Displacement Behaviour of Heavy Metals on Peat. Master's Thesis. Göteborg, Sweden : Chalmers University of Technology ; (2006).

110 Lim TC, editor. Theory and Applications in Industry, Healthcare and Defense. Boca Raton : CRC Press ; 2011.

111 Broniatowski M. Long-Chain Alkyl thiols in Langmuir Monolayers. Journal of Colloid And Interface Science. 2009;337(1):183-190.

112 Dzung NTK, Ludwig R. Calixarene-Based Molecules for Cation Recognition. Sensors. 2002;2(10):397-416.

113 Rai A, Singh A, Ahmad A, Sastry M. Role of Halide Ions and Temperature on the Morphology of Biologically Synthesized Gold Nanotriangles. Langmuir. 2006;22(2):736-741.